Signal Processing Approaches to Diagnosis of Esophageal Motility Disorders

Mani Najmabadi

A Thesis

in

the Department

of

Electrical and Computer Engineering

Presented in Partial Fulfillment of the Requirements

for the Degree of Master of Applied Science (Electrical and Computer Engineering) at

Concordia University

Montreal, Quebec, Canada

August 2008

Your file Votre référence
ISBN: 978-0-494-45496-1
Our file Notre référence
ISBN: 978-0-494-45496-1

ABSTRACT

Signal Processing Approaches to Diagnosis of Esophageal Motility Disorders

Mani Najmabadi

Esophageal Motility Disorders (EGMDs) are a group of abnormalities characterized by the muscular dysfunction of the esophagus in the transportation of food from the oral cavity to the stomach. EGMDs typically cause chronic problems and affect a vast and ever-increasing number of the global population.

The diagnosis of EGMDs mainly relies on a key test presently used to study the esophagus motility, known as esophageal manometry (EGM). EGM involves pressure measurements inside the esophagus, which provide information pertaining to its contractions. The diagnosis process is mainly based on visual inspection of the EGM test results to find certain characteristics of the manometric patterns.

There are several factors that make such inspection tedious. For instance, manometry test results are often contaminated with a considerable amount of noise, (*e.g.* noise from external environment) and artifacts, (*e.g.* respiration artifacts) leading to a longer and more complex diagnosis process. As such, the diagnosis based on visual inspection is prone to human error and demands extensive amount of expert's time.

This thesis introduces new signal processing approaches to provide an accurate means for the diagnosis of EGMDs as well as to reduce the amount of time spent on the diagnosis process. Specifically, a new technique known as wavelet decomposition (WD)

is applied to the filtering of the EGM data. A nonlinear pulse detection technique (NPDT) is applied to the de-noised data leading to extraction of diagnostically important information *i.e.* esophageal pulses. Such information is used to generate a model using a statistical pulse modeling (SPM) technique, which can classify the EGM patterns.

The proposed approaches are applied to the EGM data of 20 patients and compared with those from existing techniques. Such comparisons illustrate the advantages of the proposed approaches in terms of accuracy and efficiency.

As part of this thesis, a new circuit-based approach is proposed for the treatment of Gastroesophageal Reflux Disease (GERD), *i.e.* the most prevalent disease caused by EGMDs. The objective is to provide a framework for further research towards the implementation of the proposed approach for GERD treatment.

ACKNOWLEDGEMENTS

I would like to thank my supervisors Dr. Vijay Devabhaktuni and Dr. Mohamad Sawan for their efforts in the advancement of my education and career.

I also want to express genuine appreciation for the expert advice and council of Dr. Carlo Fallone and Dr. Serge Mayrand. Their extensive technical knowledge in gastroenterology as well as their assistance served as a backbone for this work. Additionally, this work would not have been possible without the efforts and support of my colleagues in the CAD laboratory at Concordia University. A special mention of gratitude must be made to Navid Arbabi, Farzin Manouchehri and Li Zhu for their continued support and friendship. I would also like to extend my heartfelt appreciation to my family for their ongoing guidance, support, and understanding.

Lastly, financial support received by the Regroupement Stratégique en Microsystèmes du Québec (ReSMiQ) was well appreciated and most helpful during my studies at Concordia University.

To my loving parents

Pourandokht and Bagher

TABLE OF CONTENTS

LIST OF FIGURES

LIST OF TABLES

LIST OF SYMBOLS AND ABBREVIATIONS

C	Wavelet coefficient
δ	Sampling period
E	Signal energy
ε	Sensitivity
f	Function
p_f	Falling point
p_r	Rising point
ψ	Mother wavelet
R^n	n-Dimensional space
APDR	Accurate pulse detection rate
BPSK	Binary phase shift keying
CMFB	Common mode feedback
CP	Critical point
CWT	Continuous wavelet transform
DES	Diffuse esophageal spasm
DWT	Discrete wavelet transform
ECG	Electrocardiography
EEG	Electroencephalography

EMD	Empirical mode decomposition
EGM	Esophageal manometry
EGMD	Esophageal motility disorder
GER	Gastroesophageal reflux
GERD	Gastroesophageal reflux disease
IMF	Intrinsic mode function
LDO	Low-drop-out
LES	Lower esophageal sphincter
MASI	Maximum sharpness indicator
MISI	Minimum sharpness indicator
NLEO	Nonlinear energy operator
NPDE	Normalized pulse duration error
NPDT	Nonlinear pulse detection technique
PM	Poincaré mapping
PSI	Pulse symmetry index
SBR	Signal-to-background ratio
SD	Standard deviation
SLESR	Swallow-induced lower esophageal sphincter relaxation
SPM	Statistical pulse modeling
TLESR	Transient lower esophageal sphincter relaxation
UES	Upper esophageal sphincter
VCO	Voltage controlled oscillator
WD	Wavelet decomposition

Chapter 1

Introduction

1.1 Esophageal Motility Disorders Diagnosis

Esophageal Motility Disorders (EGMDs), are a group of abnormalities originated by the muscular dysfunction of the esophagus in transportation of food from oral cavity to the stomach [1]. These disorders correspond to very common diseases such as gastroesophageal reflux disease (GERD), diffuse esophageal spasm (DES) and nutcracker esophagus that are typically chronic and life-long [2]. For instance, GERD which is a state in which the liquid content of the stomach refluxes into the esophagus affects an estimated 5-7% of the global population including men, women, and children [3]. Owing to relatively unhealthy diets and lifestyles, this percentage is even higher among the

North American population. Such diseases affect the patients' quality of life by causing problems such as heartburn, swallowing/breathing difficulties and chest pain.

Current diagnosis of EGMDs is based on a group of esophageal tests designed to examine the esophagus. The main purpose of these tests is to observe the function of the esophagus muscles regarding the food delivery. A noninvasive test presently used to study the esophagus is EGM. The EGM test essentially measures the pressure inside the esophagus, which in turn allows experts to discern vital information about the contractions of the different esophageal regions. The diagnosis process mainly involves visual inspection of these test results to find certain morphological characteristics of the manometric patterns. However, there are several factors that make such a visual inspection tedious. First, EGM data is contaminated by high-frequency noise, *e.g.* noise from external environment. Second, visual examination of EGM data involves differentiating between contractions and artifacts (*e.g.* respiration artifacts), which is prone to human error. Third, medical experts should examine each esophageal pulse/contraction and determine whether it is normal.

General solutions to overcome the above challenges can be realized by means of a computer-based implementation, with emphasis on accuracy and efficiency. Obviously, such implementation requires development of signal processing techniques for EGM data analysis, including the filtering of the noise from the raw EGM data, detection/extraction of the key information in the whole data recording and classification of the results for diagnosis.

1.2 Motivation and Objectives

The motivation behind this thesis is the desire to provide new signal processing tools to medical experts in an effort to aid in overcoming the challenges in the diagnosis of EGMDs. The main objectives are reducing the amount of time spent on the diagnosis process as well as providing an accurate means for the diagnosis of EGMDs. From a healthcare perspective, this work is highly practical as it enhances the ability of experts to diagnose disorders affecting a vast and ever-increasing number of the North American population.

1.3 Thesis Outline

This thesis proposes new signal processing-based approaches for the analysis and modeling of EGM data to assist the diagnosis of EGMDs. In addition, a new circuit-based electrical engineering approach for treatment of GERD is presented.

Chapter 2 presents an overview of the EGMDs from a medical perspective including a brief description of the esophagus anatomy, an explanation of EGMDs origin, as well as different types of diseases caused by EGMDs. Also, a brief overview of GERD as well as a short description of the relevant esophagus physiology is presented.

Chapter 3 describes a wavelet-based signal processing technique known as WD for filtering of the high-frequency noise from EGM data. The chapter begins with the background theory of an existing technique proposed for EGM data analysis known as empirical mode decomposition (EMD). The proposed WD is then described in detail.

Both the EMD and the WD are applied to the patients' EGM data and the experimental results are shown for the purpose of comparison.

Chapter 4 introduces novel approaches for detection/extraction of the diagnostically key information and model-based classification of EGM data. The relevant background theory regarding pulse detection techniques as well as a pertinent modeling technique is presented. The proposed approaches to detection/extraction and modeling of esophageal pulses are then described. The approaches are applied to the patients' EGM data and the experimental results are illustrated. Such results are compared with the results from similar existing techniques where applicable.

Chapter 5 proposes a circuit-based electrical engineering approach for treatment of GERD as the most prevalent esophageal disease caused by EGMDs. The idea for implementation of the approach using an electronic implantable device is described. Furthermore, a number of recent state-of-the-art circuits for the proposed implant structure from the existing literature are presented.

Chapter 6 contains a discussion on the thesis' contributions as well as the direction for possible future works.

Chapter 2

Esophageal Motility Disorders (EGMDs) Overview

As previously mentioned, EGMDs are identified by the muscular dysfunction of the esophagus in transporting the food from the oral cavity to the stomach. In order to understand the causes of the EGMDs, it is necessary to know the physiology of the esophagus and its function. In this chapter, a brief overview of the esophagus anatomy and its functional role is discussed. In addition, the diagnosis process of EGMDs and the corresponding challenges are described. Also presented in this chapter, is a brief background overview of GERD including its definition and causes.

2.1 The Esophagus and its Function

The esophagus is a muscular tube that has the function of transporting the food from the oral cavity to the stomach (see Figure 2.1).

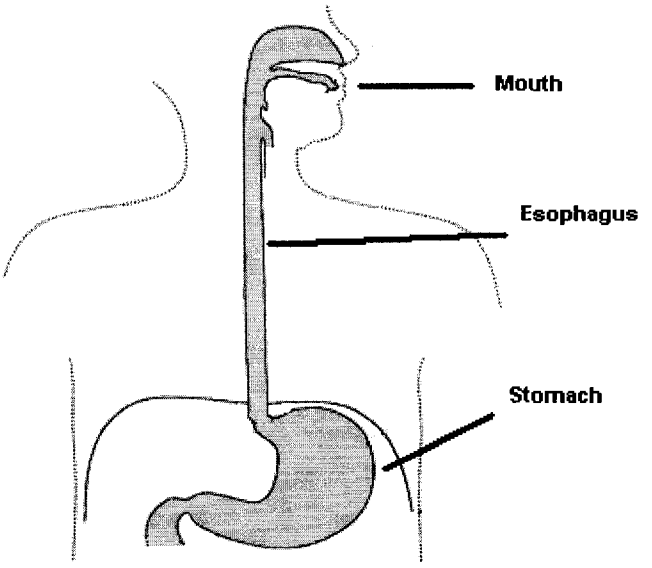

Figure 2.1 The esophagus location in human body.

In order to carry out this task safely and effectively, the esophagus is constructed as an 18 to 26 cm long hollow muscular channel with a slippery inner lining [1]. After each swallow, the food travels from mouth down to the throat and into the esophagus, passes the mid part of the esophagus and enters the stomach. During this journey, the muscles of the esophagus work together to receive food bolus in each level and push it down towards the stomach. This process is called the esophageal peristalsis. In essence, the entire esophagus wall consists of muscles that work harmoniously to transit

swallowed content to the stomach. Figure 2.2 shows an example of an esophageal peristalsis.

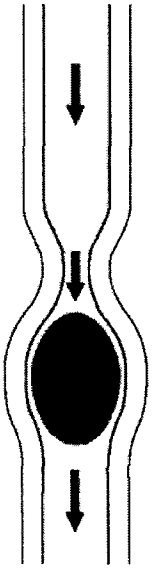

Figure 2.2 Esophageal peristalsis for transportation of food.

There are two sphincters at the beginning and the end of the esophagus that control the transition of material. The first sphincter (known as upper esophageal sphincter or UES) is located at the junction of the oral cavity and the esophagus. It controls the entrance of the esophagus and contracts unless there is a swallow event. The second sphincter (known as lower esophageal sphincter or LES) is located between the esophagus and the stomach. It controls the junction between the esophagus and the stomach and is contracted unless there is a swallow event. In every swallow process, food passes through the UES, travels along esophageal body and passes through the LES to enter the stomach. Figure 2.3 shows the locations of the esophageal sphincters in human body.

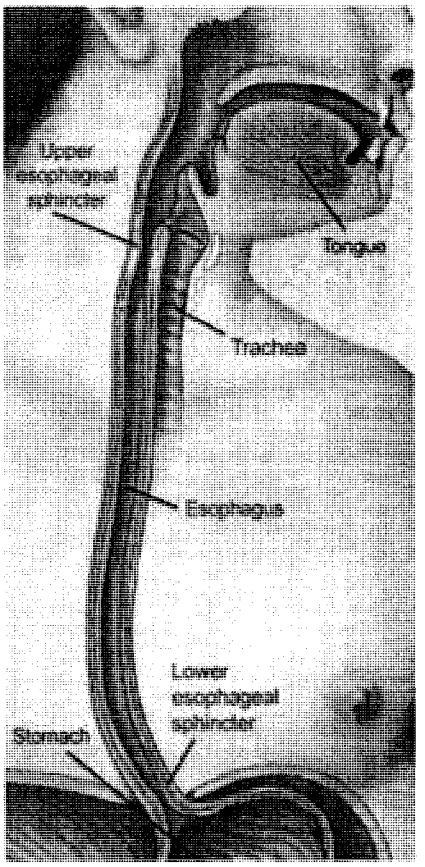

Figure 2.3 Locations of the esophageal sphincters in human body [4].

2.2 EGMDs: Definition and Classification

The delivery of food from the oral cavity to the stomach is a very complex process which involves the coordination of a set of different muscles and organs. Disruptions of this highly integrated muscular motion translate to EGMDs. Such disorders limit the delivery of food and fluid to the stomach and cause swallowing problems, chest pain, acid reflux, etc.

EGMDs are classified based on the type of abnormality which causes the disruption in esophagus function [2]. Generally, these abnormalities are: (i) uncoordinated contractions, (ii) hyper contractions, (iii) hypo contractions, and (iv) inadequate sphincter relaxations. Various disorders and diseases are originated from such categories of abnormalities. In the following section, a brief overview of the most common disorders and diseases initiated from esophagus abnormalities is presented.

2.3 Common Esophageal Motility Disorders and Diseases

In order to know the importance of EGMDs and their impact on society's health, a brief overview of the most prevalent disorders and diseases related to EGMDs is presented in this section.

2.3.1 Gastroesophageal Reflux Disease (GERD)

GERD, generally known as acid reflux, is a state in which the liquid content of the stomach refluxes into the esophagus. The acidic nature of the liquid has the potential to damage the sensitive lining of the esophagus, causing esophagus inflammation, known as esophagitis. GERD is a chronic, and in most cases life-long disease, which can result in possible swallowing and breathing problems or even esophageal cancer in extreme cases. GERD is caused by the dysfunction of the LES as a barrier to reflux of acidic content of the stomach to the esophagus. It is estimated that GERD currently affects an estimated 5-7% of the world's population. Owing to relatively unhealthy diets and lifestyles, this percentage is even higher in the North American population (approximately 22 million people in North America suffer from GERD) [3].

2.3.2 Achalasia

Achalasia is an EGMD of unknown cause characterized by the absence of peristalsis in esophageal body and impaired relaxation of the LES. As a result, patients with achalasia usually suffer from swallowing difficulties and weight loss. Although it is not a very common disease, it is frequent enough to be considered as an important EGMD. Achalasia is a disease that occurs with equal frequency between men and women. There are, however, striking international differences with the disease. Achalasia is more common in North America, north-western Europe and New Zealand [2].

2.3.3 Diffuse Esophageal Spasm (DES)

DES is an EGMD of unknown cause characterized by uncoordinated spastic activity in the smooth muscle portion of the esophagus. DES is manifested clinically by episodes of swallowing difficulty and chest pain. Such a pain can mimic the angina of coronary artery disease which is critical due to the fact that DES patients are typically older than 50 years of age. DES occurs with equal frequency between men and women. DES is more common in North America compare to the rest of the world.

2.3.4 Nutcracker Esophagus

Nutcracker Esophagus is a condition in which the swallow induced peristaltic waves in the esophageal body have higher amplitudes compared to normal levels. Therefore, patients diagnosed with Nutcracker Esophagus suffer from severe chest pain and swallowing difficulties to both solid and liquid foods. Nutcracker esophagus can affect people of any age, but is more common in the 6th and 7th decades of life.

2.4 Diagnosis of EGMDs and the Role of EGM

The diagnosis of EGMDs is a complex process which involves a number of tests to examine the esophagus and its function. The most important test for assessment of esophagus is EGM. As mentioned, EGM involves pressure measurements inside the esophagus, which provide information in terms of contractions of the esophagus [1]. This is due to the fact that any abnormality in esophagus function manifests itself in pressure dynamics inside the esophagus. Such measurements, *i.e.*, the recorded pressure waveforms, are reviewed by medical experts, in order to qualify/quantify the wave morphologies leading to classification of normal and abnormal patterns.

There exist a number of EGM procedures which medical experts employ depending upon the symptoms of the patient. These procedures are (i) sphincter examination/profiling and (ii) esophageal body examination. The former is mainly employed for examination of the LES in diagnosis of GERD or examination of the UES in diagnosis of swallow related disorders in the pharynx area. The latter is mainly employed for diagnosis of motility disorders in the esophageal body such as DES and Nutcracker Esophagus. A brief description of such procedures is presented in the following sections.

2.4.1 Manometry Procedure for Sphincter Examination/Profiling

EGM for sphincter examination/profiling is performed while the patient is awake, alert, and in a supine position. The procedure takes about 40 minutes and the patient should have fasted for six hours [2]. An esophageal motility catheter, which is a

flexible/soft tube containing micro-transducers for pressure measurements is used. The catheter is slowly passed into the esophagus through the nose and throat of the patient. Profiling of the sphincter (*i.e.* LES or UES) is done using the station pull-through technique, which involves a slow and step-wise withdrawal of the catheter. The catheter is moved in 0.5cm steps and is held at each position/station long enough so as to obtain a stable pressure reading. Once the pressure data is recorded, the results are saved on a machine or printed on to a paper. An example of the manometry results for LES profiling from a patient is shown in Figure 2.4. The LES high pressure zone is labelled in the figure.

2.4.2 Manometry Procedure for Esophageal Body Examination

EGM for esophageal body examination is performed while the patient is awake, alert, and in a supine position. The procedure takes about 40 minutes and the patient should have fasted for at least six hours. Medications that may potentially alter normal esophageal function must be discontinued at least 24 hours before the procedure [2]. An esophageal motility catheter, which is a soft tube containing micro-transducers, is used. The catheter is slowly passed into the esophagus through the nose and throat of the patient. The patient is usually asked to swallow saliva (*i.e.* a dry swallow) or water (*i.e.* a wet swallow). The esophagus muscles normally contract from the top portion of the esophagus and progress in an orderly sequence to the bottom portion of the esophagus. Resulting pressure changes from esophageal contractions are recorded. The recordings are in the form of tracings in time-domain. Sampling rate and other signal specifications

are adjusted by the medical doctor. An example of a 15s manometry results for esophageal body examination from a patient is shown in Figure 2.5.

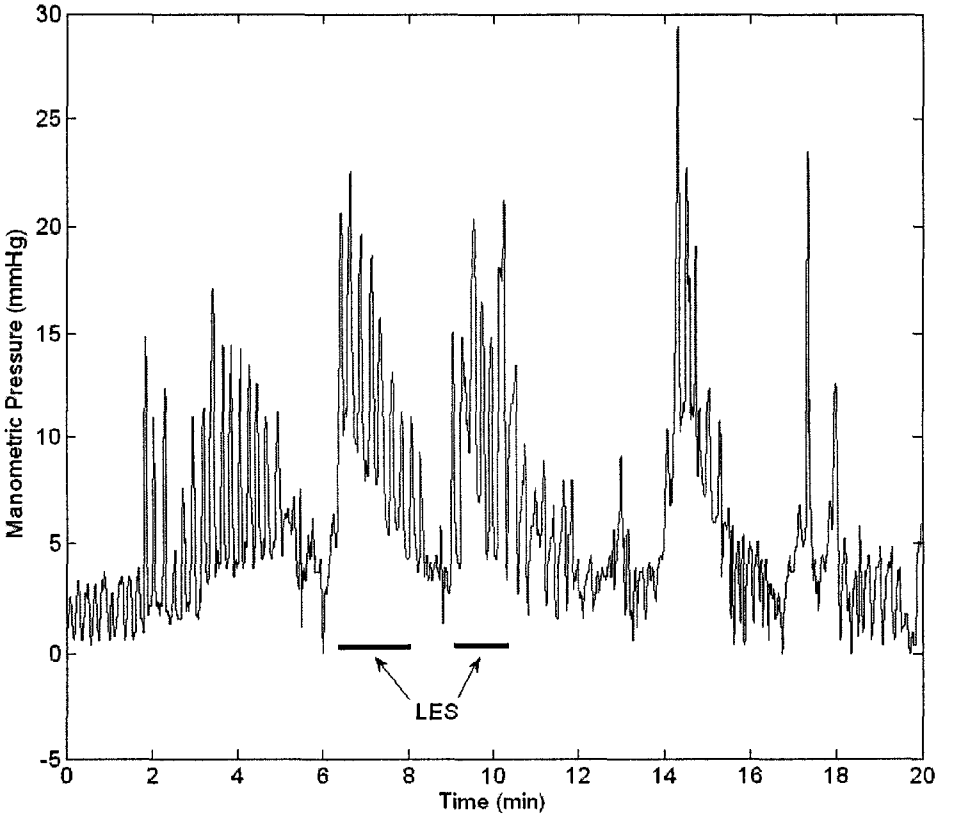

Figure 2.4 An example of the manometry results for LES profiling.

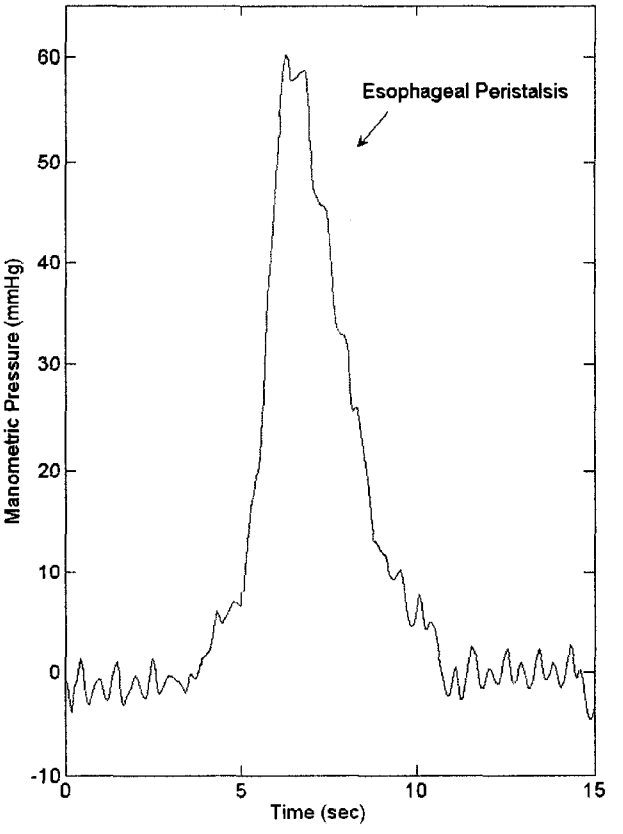

Figure 2.5 An example of the manometry results for esophageal body examination.

2.5 Challenges in Diagnosis of EGMDs Using EGM

As previously mentioned, EGM involves pressure measurements inside the esophagus, which provide information in terms of contractions of the esophagus. These measurements, *i.e.*, the recorded pressure waveforms, are reviewed by medical experts, in order to qualify/quantify the wave morphologies leading to classification of normal and abnormal patterns. Similar to other biological signals, *e.g.* electrocardiography (ECG) and electroencephalography (EEG), EGM signal/wave analysis by medical experts highly relies on visual inspection. However, there are several factors that make visual inspection

tedious. First, EGM data is contaminated by high-frequency noise, *e.g.* noise from external environment. Second, manual examination of EGM data involves differentiating between contractions and artifacts (*e.g.* respiration artifacts), which is prone to human error. Third, medical experts should examine each esophageal pulse/contraction and determine whether it is normal. As such, accurate diagnosis based on visual inspection demands extensive amount of expert's time, and such inspection can be even more challenging in the case of 24-hour EGM data monitoring.

2.6 Computer Aided Solutions for EGMDs Diagnosis Using EGM

A general solution to the mentioned problems is to filter the high-frequency noise, browse through the de-noised EGM data to extract critical data portions/segments, and compare these portions with standard cases for diagnosis. The above solution can be realized by means of a computer-based implementation using signal processing methods, with emphasis on accuracy and efficiency. Obviously, such implementation requires development of an algorithm for EGM data analysis, which involves three specific tasks, namely, i) filtering of high-frequency noise from raw EGM data, ii) detection/extraction of diagnostically important segments from the EGM recordings, and iii) development of a convenient computational model that facilitates differentiation between normal and abnormal patterns.

In chapters 3 and 4, the proposed signal processing techniques for implementation of the above tasks are presented. The following section is dedicated to a background overview of GERD, necessary for the GERD treatment approach described in chapter 5.

2.7 GERD Overview

Gastroesophageal Reflux Disease (GERD), generally known as acid reflux, is a state in which the liquid content of the stomach refluxes into the esophagus [3]. The acidic nature of the liquid has the potential to damage the sensitive lining of the esophagus, causing esophagus inflammation, known as esophagitis. GERD is a chronic, and in most cases life-long disease, which can result in possible swallowing and breathing problems or even esophageal cancer in extreme cases. It is estimated that GERD currently affects an estimated 7% of the global population. The widespread effect of this disease reflects the need to develop effective diagnosis and treatment methods compared to those presently available.

Current diagnosis of GERD involves a set of esophageal tests designed to examine the esophagus. One of the key tests presently used to study the esophagus in GERD diagnosis is EGM. EGM allows experts to obtain vital information about the amplitude and coordination of esophageal contractions especially in the LES region.

Medical treatment of GERD is a complicated process and is based on symptoms presented along with organ damages [2]. Less invasive treatments involve life-style changes such as alteration of eating and sleeping habits. More severe cases are treated with prescription drugs such as antacids to control the reflux. More advanced and invasive GERD management methods include surgical and endoscopic techniques [3]. Despite the numerous existing techniques for GERD treatment, research towards an effective cure for GERD has continued unabated.

2.8 Cause of GERD

The backward flow of gastric content into the esophagus, that is, gastroesophageal reflux (GER), is up to a certain extent a normal physiological phenomenon [1]. When the threshold of normality is surpassed, GER may induce inflammatory changes of the esophageal inner lining due to exposure from stomach contents. These contents (*i.e.* acid and enzymes) can damage the esophagus leading to symptoms such as chest pain, swallowing and breathing problems.

There is a natural anti-reflux barrier in the junction of the esophagus and the stomach preventing the flow of stomach contents into the esophagus. This natural barrier is the LES. LES is in fact a muscle that acts as a valve at the opening of stomach. The failure of the LES to prevent the acid flow from the stomach to the esophagus causes GER episodes and overtime results in GERD. The location of the LES is demonstrated in Figure 2.6. A brief description of the LES is presented in the following section.

2.8.1 Lower Esophageal Sphincter (LES)

The LES involves 3 to 4 cm of the esophagus right above the stomach [1]. Resting LES pressure ranges from 10 to 30 mmHg (or Torr). A minimum of 5 to 10 mmHg is necessary to prevent GER from stomach to the esophagus. The LES has the duty of maintaining a high pressure almost at all times except an event of a swallow event. There is considerable daytime variation in LES pressure; it is lowest after meals and highest at night. It is also influenced by circulating hormone related foods (particularly fat) as well as a number of drugs [1] [2]. It is to note that the diaphragm (see Figure 2.6), provides

external squeeze to the LES, contributing to resting pressure during inspiration and augmenting LES pressure during periods of increased abdominal pressure such as coughing, sneezing, or bending. Diaphragm contractions impose rhythmic pressure increases of about 5 to 10 mmHg on the LES pressure assuring the LES function.

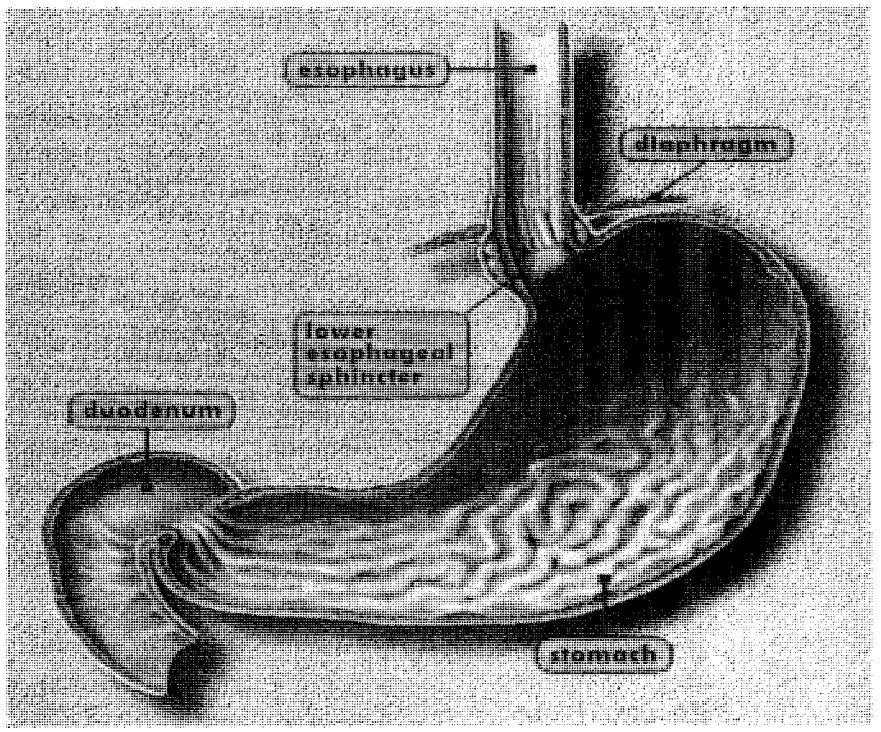

Figure 2.6 LES location at the junction of the esophagus and the stomach [5].

LES is controlled directly by the brain and receives its control signals through one of the most important nerve branches known as Vagus nerve. Vagus nerve is the only nerve that initiates in the brainstem and controls most of the vital organs such as heart, liver and kidneys. It regulates both the inhibitory (relaxation) and the excitatory (contraction) responses of the LES.

As mentioned, LES is the barrier to acid reflux from stomach to esophagus and its dysfunction results in GERD. However, it has not been mentioned as to which LES characteristic corresponds to GERD origin. Therefore, a question may arise: Is the absence of LES tone/pressure the cause of GERD or there are other factors?

In order to find the answer to the above question one should study the conditions in which GER is most likely. In the following section, the mechanisms of reflux are explained.

2.8.2 Mechanisms of Reflux

2.8.2.1 Transient Lower Esophageal Sphincter Relaxations (TLESR)

A TLESR is a relaxation of LES that is not initiated by a swallow. TLESRs are the most frequent mechanisms for reflux in patients with sufficient sphincter pressure. Such LES relaxations occur independently of swallowing, are not accompanied by esophageal peristalsis, usually persist longer than 10 seconds and are accompanied by inhibition of diaphragm pressure. Importantly, TLESRs account for 50% to 80% in GERD patients.

2.8.2.2 Swallow-Induced Lower Esophageal Sphincter Relaxations (SLESR)

A SLESR is a relaxation of LES that is initiated by a swallow in order to allow food to enter the stomach. About 5% to 10% of reflux episodes occur during swallow-induced LES relaxations. Most episodes are associated with defective or incomplete peristalsis. During a normal SLESR, reflux is uncommon due to the factors; (i) the

diaphragm does not relax (ii) the duration of SLESRs is really short (around 5 seconds) (iii) reflux is prevented by the oncoming peristaltic wave.

2.8.2.3 Hypotensive (Low-Pressure) Lower Esophageal Sphincter

GER can occur in the context of hypotensive LES by either strain-induced or free reflux. Strain induced reflux occurs when a relatively hypotensive LES is overcome and blown open by normal events such as coughing or bending over. Free reflux is characterized by a fall in esophageal ph caused by extremely low LES pressure. Reflux due to a low or absent LES pressure is uncommon.

2.9 A Potential Solution for GERD Treatment

As explained in the previous section, acid reflux can occur during different mechanisms which may result in GERD. Therefore, GERD is considered as a multi-factorial disease *i.e.* various factors can cause GERD. However, the common feature in all GERD cases is the LES failure to stay contracted in the absence of a swallow. As such, a general solution for GERD treatment should involve the control of LES in order to assure its contraction at appropriate times. In chapter 5, an engineering approach based on electrical stimulation of the LES using neurostimulation techniques for GERD treatment is presented.

2.10 Summary

In this chapter, function of the esophagus as well as a brief overview of the EGMDs has been presented. Also, the challenges in EGMDs diagnosis along with the

proposed signal processing-based solutions have been discussed. In addition, a brief overview of GERD as the most important disease caused by EGMDs, has been described.

Chapter 3

De-noising of EGM Data for EGMDs Diagnosis

As discussed in the previous chapters, there are certain facts that make the EGM-based diagnosis of EGMDs challenging. The primary fact is that the EGM data is usually contaminated by noise. Such noise includes components with much higher frequency compared to the frequency of esophageal movements and contractions. The potential sources of noise are external environment (*e.g.* patient's body movements) or the EGM test equipment. Such noise can make the diagnosis tedious since it may distort the esophageal waveforms. Therefore, there is a need for a suitable filtering technique to remove the high frequency noise from EGM data.

It is to be noted that raw manometric data exhibits discontinuities and sharp peaks due to natural pressure fluctuations in the esophagus. Therefore, typical filtering techniques may not be appropriate options. This is due to the fact that the resulted filtered signal using these techniques may fail to follow sharp peaks and rapid changes of the original signal. Recently, a signal processing technique referred to as Empirical Mode Decomposition (EMD) has been proposed for the analysis of manometric data [6].

In this chapter, an overview of EMD as the existing technique for analysis of EGM data in the signal processing literature is presented. The proposed technique, *i.e.* WD, for de-noising of EGM data is then described in detail. Both the EMD and WD are applied to the patients' EGM data and the experimental results are presented for comparison.

3.1 Empirical Mode Decomposition (EMD)

The EMD is a general signal processing method for analyzing nonlinear and non-stationary time series. EMD was initially proposed for the study of ocean waves, and found pressing applications in biomedical engineering [6]. The fundamental idea of EMD is to decompose a signal into a finite and often small number of intrinsic mode functions (IMFs). An IMF is defined as any function having the number of extrema and the number of zero-crossings equal (or differing at most by one), and also having symmetric envelopes defined by the local minima, and maxima respectively. The major advantage of EMD is that the IMFs are derived directly from the signal itself. Therefore, the analysis is

adaptive, in contrast to Fourier analysis, where the basis functions are linear combinations of fixed sinusoids.

3.1.1 EMD Theory and Algorithm

The principle of EMD is to decompose a signal into a sum of oscillatory functions, namely IMFs, that: i) have the same numbers of extrema and zero-crossings or differ at most by one; and ii) are symmetric with respect to local zero mean. With these two requirements, the instantaneous frequency of an IMF can be well defined.

EMD decomposes a given signal into a set of IMFs with discrete frequencies. Decomposition is accomplished by empirically identifying the physical time-scales fundamental to the data/signal. These time-scales are the time-fragments between consecutive maxima or minima. Each IMF satisfies the criteria of having a zero mean for its upper/lower envelopes. The procedure for determining IMFs includes finding upper/lower envelopes (x_{up}/x_{low}) of the signal $x(t)$ by connecting maxima/minima points via cubic splines and then subtracting the mean of the above-said envelopes from the signal *i.e.*

$$h_{11}(t) = x(t) - (x_{up}(t) + x_{low}(t))/2. \tag{3.1}$$

Treating $h_{11}(t)$ as the original signal and using (3.1), we evaluate $h_{12}(t)$. In an iterative fashion, we continue to evaluate $h_{13}(t)$, ..., $h_{1p}(t)$ and so forth. The procedure terminates when the mean of the envelopes of $h_{1p}(t)$ becomes zero, providing the first IMF *i.e.* $I_1(t) = h_{1p}(t)$. Residue $r_1(t) = x(t) - I_1(t)$ is then used as new data and the above

procedure is repeated resulting in subsequent IMFs $I_2(t) = h_{2p}(t)$, $I_3(t) = h_{3p}(t)$, and so forth, assuming p to be a variable index. The EMD approach terminates when the difference between two consecutive IMFs is equal to a small value (typically in the 0.2-0.3 range).

In principle, the original signal $x(t)$ can be reconstructed as

$$x(t) = \left\{ \sum_{i=1}^{N} I_i(t) \right\} + r_N(t). \tag{3.2}$$

In (3.2), N is the number of IMFs, $I_i(t)$ is the i^{th} IMF, and $r_N(t)$ is the residue when the EMD terminates. Since each IMF corresponds to a specific frequency component of $x(t)$, partial addition of the IMFs *i.e.*

$$\hat{x}(t) = \sum_{i=j}^{k} I_i(t), \tag{3.3}$$

results in a filtered signal. In (3.3), $j,k \in \{1,...,N\}$ and $j \le k$. It is to be noted that de-noising of the original signal can be achieved by adding the low-frequency IMFs.

3.2 Wavelet Decomposition (WD)

Wavelet decomposition is gaining attention as a novel signal processing tool for analyzing nonlinear time-series. Compared to traditional Fourier transform, wavelet transform better represents functions exhibiting discontinuities and sudden changes. As such, wavelet-based techniques are strong candidates for the analysis of bio-signals (*e.g.* gastric and esophageal signals), in which, sudden changes and sharp peaks are likely [7] [8]. A brief overview of wavelet theory and WD is presented in this section.

3.2.1 Wavelets and the Wavelet Transform

A wavelet is a mathematical function used as a basis to divide a given function or continuous-time signal into different frequency components. A wavelet transform is the representation of a function by such wavelets. The wavelets are scaled (stretched/compressed over time-axis) and positioned (shifted over time-axis) copies of a finite-length waveform known as the mother wavelet. Similar to the Fourier transform in which a signal is represented by sum of sine waves, in wavelet transform a signal is represented by sum of scaled and shifted mother wavelets. There are different types of mother wavelets developed for various applications. Figure 3.1 illustrates some of the most popular and widely used mother wavelets.

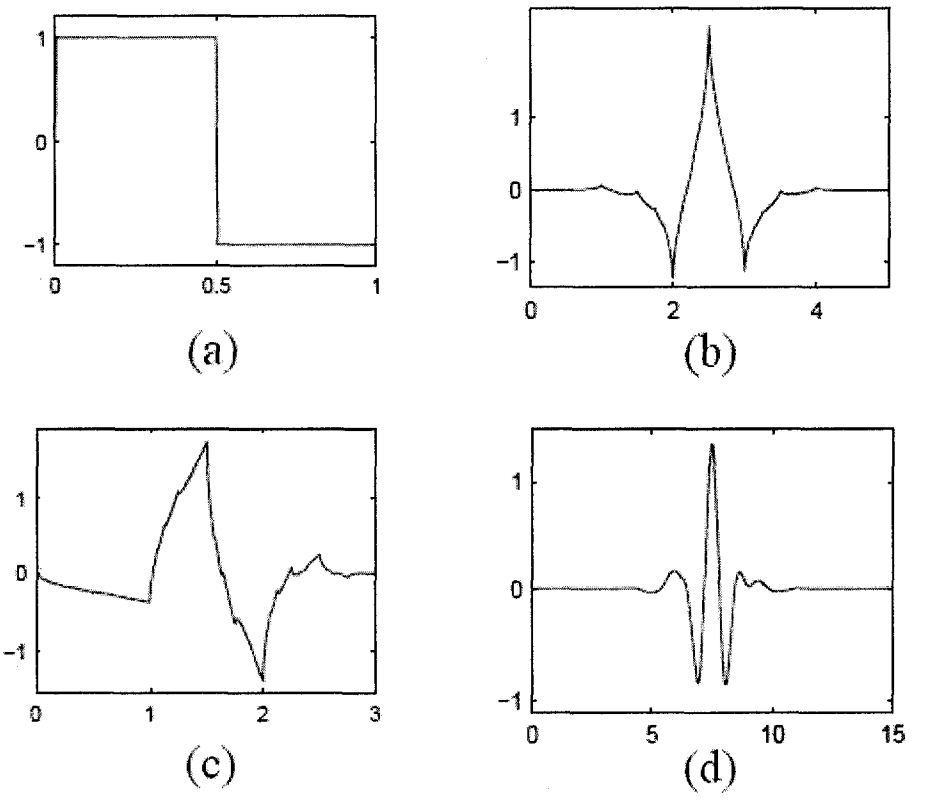

Figure 3.1 A sample group of widely used mother wavelets: (a) Haar, (b) Biorthogonal, (c) Daubechies, (d) Symlet [9].

Wavelet transforms have advantages over traditional Fourier transforms for representing functions that have discontinuities and sharp peaks, and for accurately deconstructing and reconstructing finite, non-periodic and non-stationary signals. This is due to the fact that in wavelet transform a signal is analyzed by a group of wavelets with limited length, (thus suitable for analyzing local variation of the signal) which are scaled in order to match the original signal frequency.

3.2.2 Wavelet Transform Algorithm

Wavelet transform breaks down a given signal to a group of functions known as wavelets. In this section a brief conceptual description of the general algorithm used in wavelet analysis is presented through 5 simple steps. For simplicity, the continuous-time case is described here.

The continuous wavelet transform (CWT) is the sum over all time of the signal multiplied by scaled, shifted versions of the wavelet. This process produces wavelet coefficients that are a function of scale and position.

Step1: Choose a mother wavelet and compare it to the first portion of the original signal.

Step2: Calculate a numerical value, *e.g.* coefficient *C*, which represents the similarity/correlation between the signal portion and the wavelet. The higher the *C*, the more similar is the wavelet to the original signal.

Step3: Move on to the next portion and repeat the steps 1 and 2 and calculate the coefficients, *i.e. C*s until the end of the signal.

Step4: Scale/stretch the wavelet in order to obtain the new wavelet (*i.e.* still from the same family) and repeat the steps 1 to 3 to calculate all the *C*s for the scaled wavelet.

Step5: Repeat the steps 1 to 4 for all the scales *i.e.* scaled wavelets.

Figure 3.2 illustrates the above process in CWT. Having calculated the *C*s using the above procedure, the original signal can be presented by means of a set of *C*s along with the corresponding wavelet.

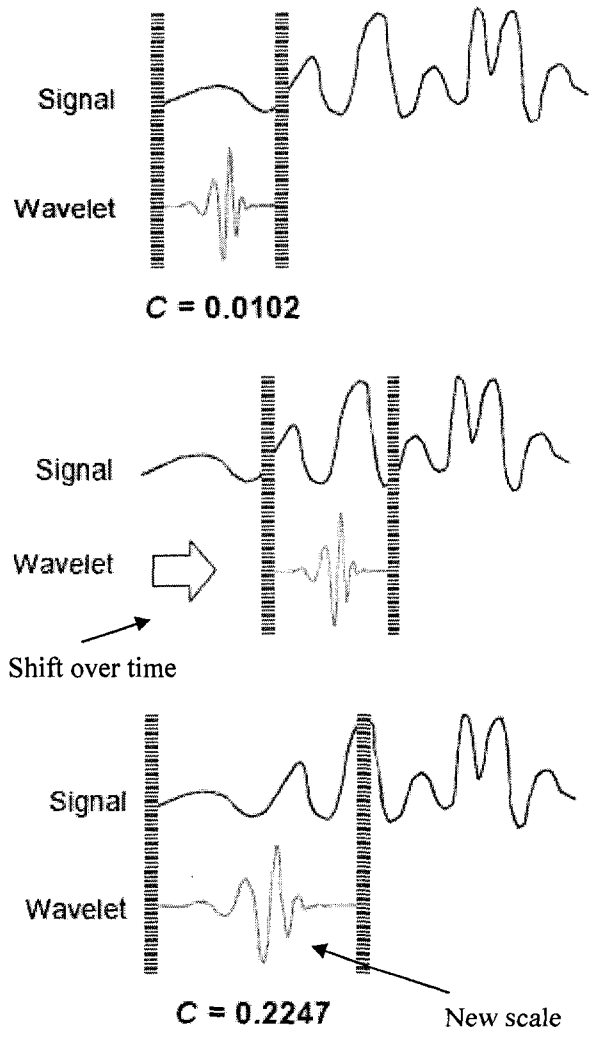

Figure 3.2 An illustration of CWT realization for a random signal [9].

It is to be noted that any signal processing performed on a computer using real-world data must be performed on a discrete signal, (*i.e.* on a signal that has been measured at discrete times) using the discrete wavelet transform (DWT). Therefore a question may arise regarding the difference between the CWT and DWT. The main factor that differentiates the CWT from DWT is the set of scales and positions at which it

operates. Unlike the DWT, the CWT can operate at every scale, from that of the original signal up to some maximum scale that you determine by trading off your need for detailed analysis with available computational horsepower. The CWT is also continuous in terms of shifting: during computation, the analyzing wavelet is shifted smoothly over the full domain of the analyzed function.

3.2.3 WD for EGM De-noising

In this section a brief overview of the WD for filtering of EGM data is presented [9]. CWT of a given signal $x(t)$ can be expressed as

$$\gamma(s,\tau) = \int x(t)\psi^{*}_{s,\tau}(t)dt\,. \tag{3.4}$$

In (3.4), s and τ denote scale and position parameters, and $\psi^{*}_{s,\tau}(t)$ is the complex conjugate of $\psi_{s,\tau}(t)$ given by

$$\psi_{s,\tau}(t) = \frac{1}{\sqrt{s}}\psi\left(\frac{t-\tau}{s}\right). \tag{3.5}$$

It is to be noted that $\psi(t)$ is a user-defined mother wavelet, and its selection depends upon the shape of the original signal. The inverse wavelet transform can be expressed as

$$x(t) = \iint \gamma(s,\tau)\psi_{s,\tau}(t)d\tau ds\,. \tag{3.6}$$

In the discrete form, we define

$$\psi_{i,j}(n) = \frac{1}{\sqrt{2^i}}\psi\left(\frac{n - j2^i}{2^i}\right), \tag{3.7}$$

where n, i, and j represent sample index, decomposition index and position index along the time-axis respectively. Substituting (3.7) in (3.4), coefficients $\gamma(i,j)$ can be evaluated for different i and j. In theory, discrete signal $x(n)$ can be re-constructed as

$$x(n) = \sum_{i\in I}\sum_{j\in J}\gamma(i,j)\psi_{i,j}(n)\,, \tag{3.8}$$

where I and J are index sets. From a signal decomposition perspective, the corresponding WD functions can be evaluated as

$$C_i(n) = \sum_{j\in J}\gamma(i,j)\psi_{i,j}(n)\,. \tag{3.9}$$

Since each C_i corresponds to a specific frequency component of $x(n)$, partial addition of the WD functions, *i.e.*

$$y(n) = \sum_{i \in \hat{I}} C_i(n), \tag{3.10}$$

where $\hat{I} \subset I$, results in a filtered biomedical signal. In other words, de-noising of the given signal can be achieved by adding the low-frequency C_is. The WD approach is applied to the de-noising of raw EGM data.

3.3 Experimental Results

In this section, the simulation results of the EMD and the WD are presented. Both the techniques are applied to the real EGM data from patients and the results are compared in order to highlight the advantages of the WD over the EMD. The presented manometry test results are obtained using the LES profiling procedure as part of the GERD diagnosis. The sampling rate in the experiments is chosen to be 6 Hz.

3.3.1 Application of EMD to EGM De-noising

EMD reviewed in section 3.1 is applied to the patient's data. The original signal is decomposed into a set of IMFs using an in-house program developed in *MATLAB*. EMD approach terminated after evaluating N = 17 IMFs, shown in Figure 3.3. De-noising of the signal is performed through a partial addition of the IMFs *i.e.* only low-frequency IMFs are considered in the summation of (3.3). The de-noised signal (see Figure 3.4) is easy-to-analyze; however, it does not accurately detect sharp peaks and rapid changes.

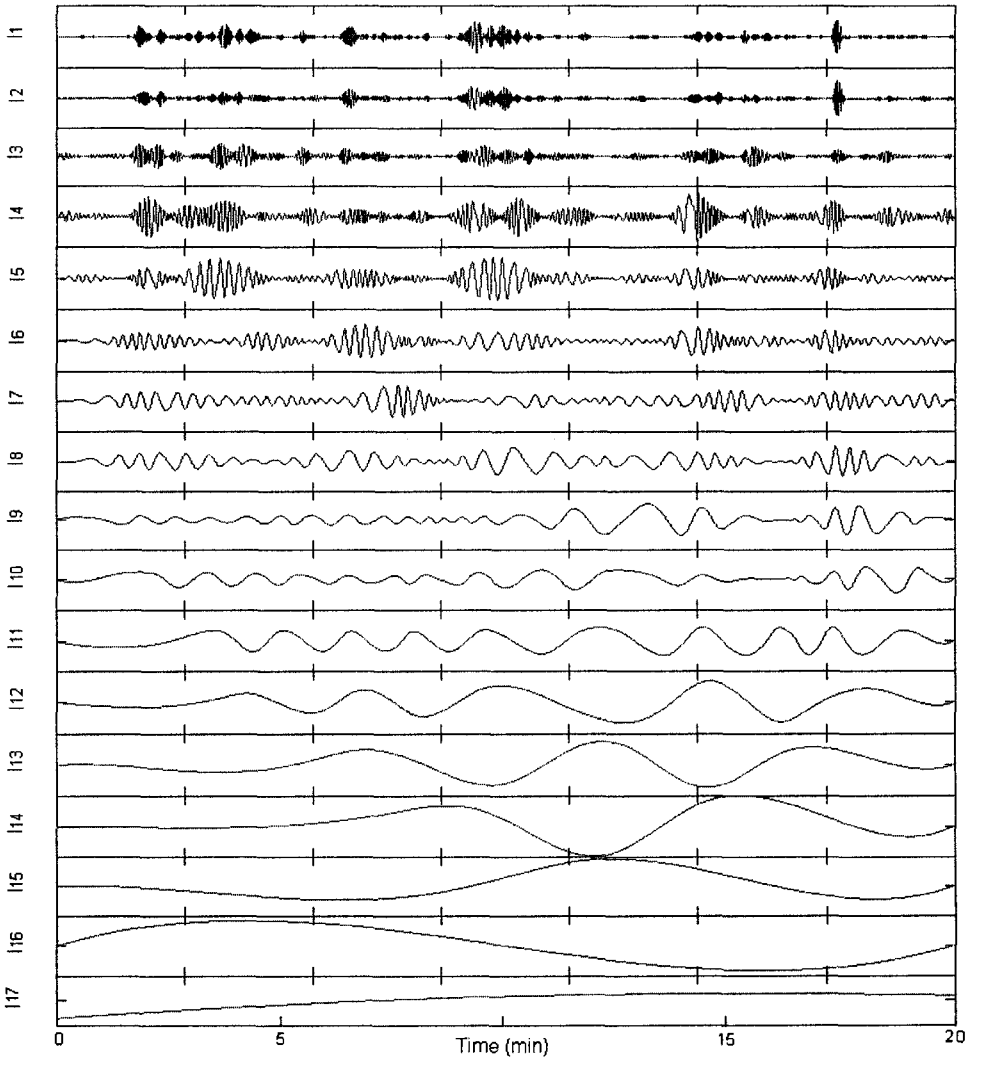

Figure 3.3 IMFs evaluated using the EMD.

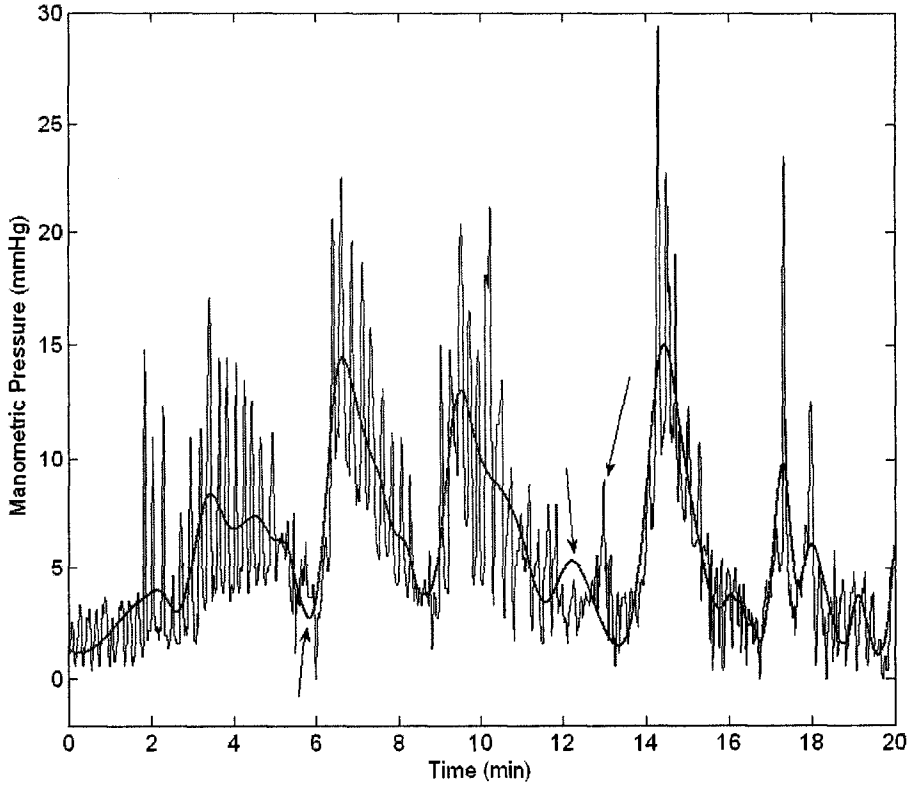

Figure 3.4 Original manometric data and the de-noised pressure signal using the EMD approach.

3.3.2 Application of WD to EGM De-noising

WD introduced in section 3.2 is applied to the patient's data. For this purpose, built-in functions of *MATLAB* are used. Considering the time-domain behaviour of the pressure signal, index i is chosen to be 15. Owing to the shape of the signal, mother wavelet "sym3" shown in Figure 3.5 is picked. Resulting wavelets (C_is) are shown in Figure 3.6.

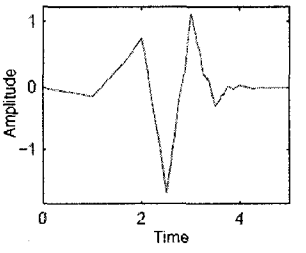

Figure 3.5 Mother wavelet 'sym3' used in the WD approach.

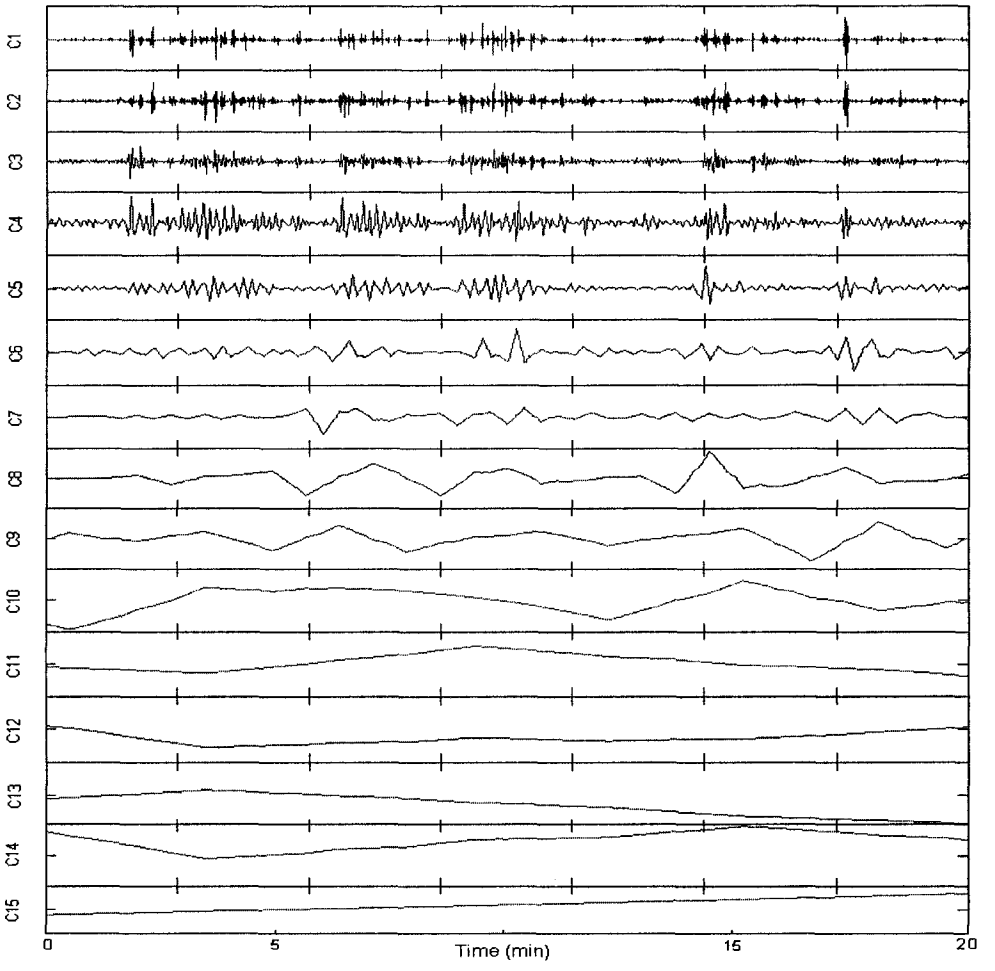

Figure 3.6 WD functions *i.e.* C_is evaluated using the WD approach.

Typically, esophageal movements and contractions correspond to a frequency range less than 0.1Hz. As such, de-noised pressure signal is obtained using (3.10) with $\hat{I} = \{5, 6, 7, \ldots, 10\}$. The de-noised signal (see Figure 3.7) does not miss sharp peaks and sudden changes present in the original signal. In addition, there is no obvious phase difference between the original and de-noised signals.

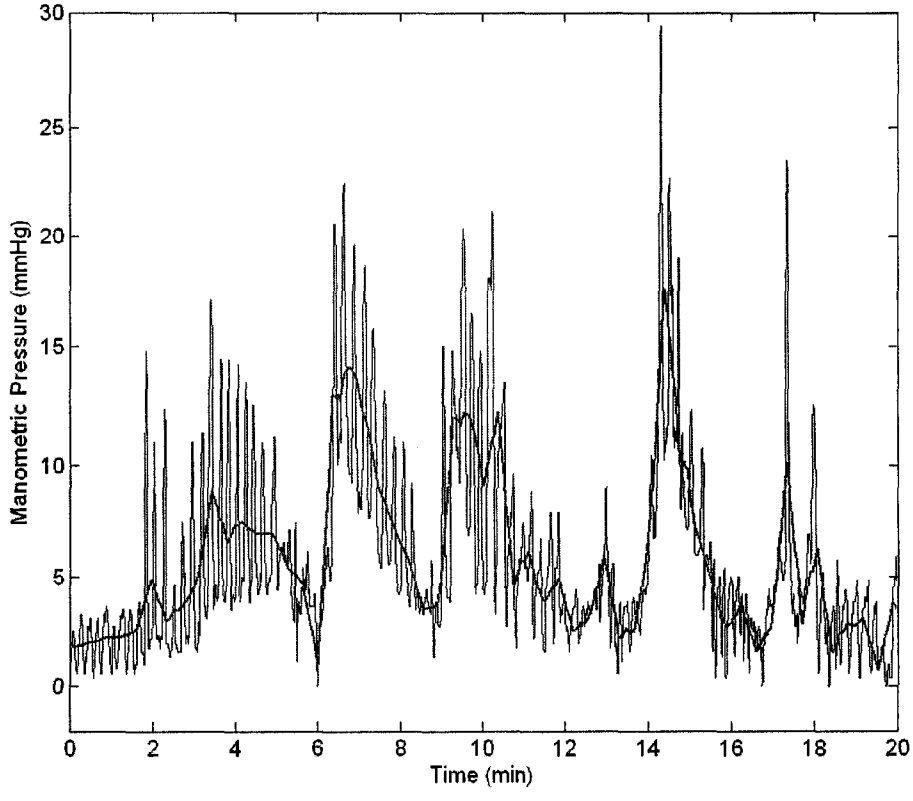

Figure 3.7 Original manometric data and the de-noised pressure signal using the WD approach.

3.3.3 Comparison of EMD and WD in EGM De-noising

For the purpose of comparison, de-noised signals from both EMD and WD approaches along with the raw signal are shown in Figure 3.8. In general, both methods

seem to provide a smooth de-noised signal. However, a close inspection of the results could lead to interesting observations. De-noised signal from the WD approach is able to detect/retain all the sharp changes in the original signal, which is not the case with the de-noised signal from the EMD approach. There is a phase difference between the de-noised signal from EMD and the given signal.

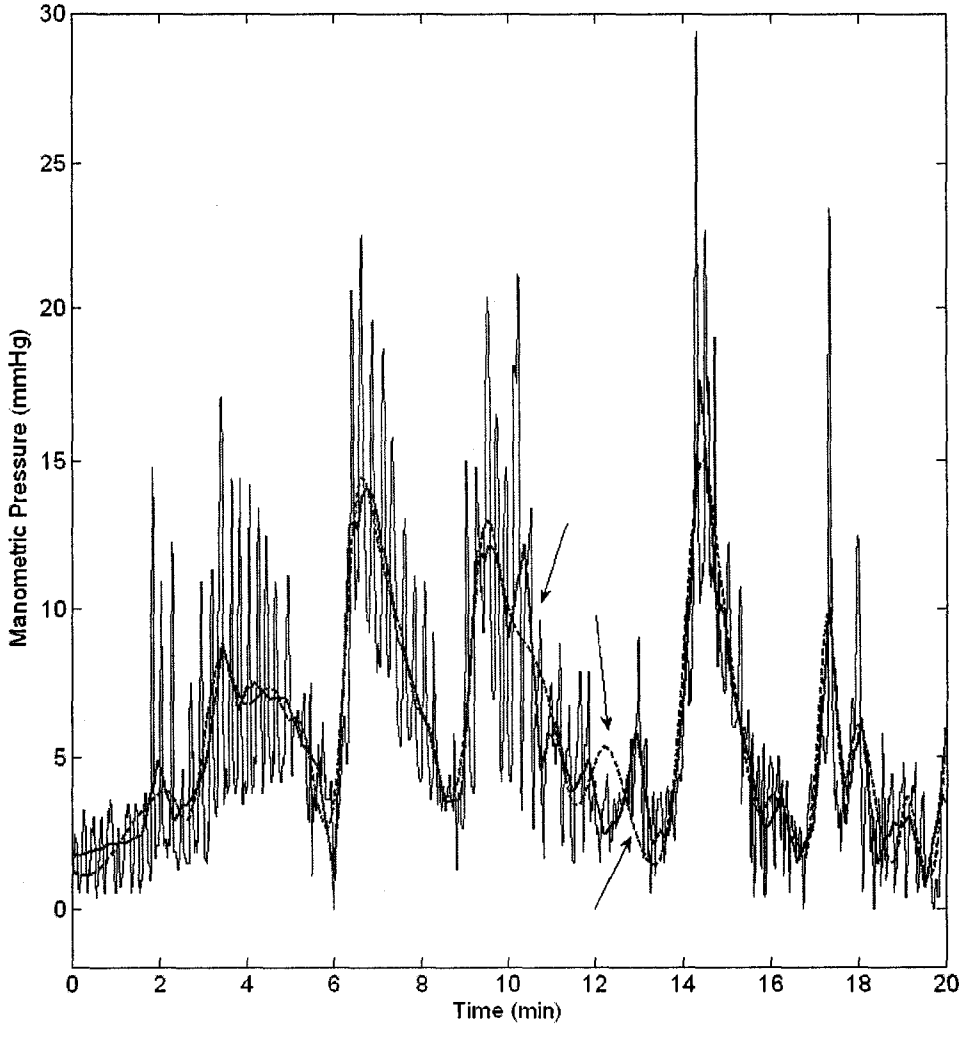

Figure 3.8 Comparison of the original manometric data, the de-noised pressure signal using the EMD approach and the de-noised pressure signal using the WD approach.

A comparison in terms of number of decompositions/coefficients, CPU-time, and signal-to-background ratio defined as

$$SBR = \frac{\sum_{i=1}^{n} (\hat{x}(t_i))^2}{\sum_{i=1}^{n} (x(t_i))^2}, \tag{3.11}$$

is presented in Table 3.1. In the above definition of *SBR*, $\hat{x}(t_i)$ is the filtered signal and n represents the total number of samples.

TABLE 3.1
COMPARISON OF EMD AND WD APPROACHES

Decomposition Method	**No. of Decompositions**	**CPU-Time**	***SBR***
EMD	17	75s	0.85
WD	15	0.5s	0.97

3.4 Summary

In this chapter, a wavelet-based decomposition approach has been applied to the filtering of esophageal manometric data critical to EGMDs diagnosis. For comparison, the WD approach and a recent approach (*i.e.* EMD) have both been applied to the patients' data. The WD approach is better in terms of accuracy, and the corresponding de-

noised signal conveys relatively better information. In addition, the WD approach requires less CPU-time

Chapter 4

Analysis and Modeling of EGM Data for EGMDs Diagnosis

As discussed in the previous chapters, there are certain factors that make the EGM-based diagnosis of EGMDs challenging. In chapter 3, WD was presented as an effective tool for EGM data de-noising. In this chapter the other challenges are addressed through signal processing techniques for detection/extraction of diagnostically key information and generation of a computational model for classification of EGM patterns benefiting the EGMDs diagnosis.

Subsequent to high-frequency noise filtering, detection and extraction of critical EGM data segments is important for EGMDs diagnosis. It is to be noted that the primary wave morphologies to be detected and extracted from the EGM data are the esophageal pulses or contraction waves. For biomedical pulse/spike detection, several techniques have been proposed [10]-[12], although not specifically for the EGM data. Some of the early works based on the concept of sharpness [10], had limited success. Some of the more recent techniques are based on time-frequency analysis [13] and spectrum analysis [14]. In the case of EGM data, not much research has been reported thus far, and this is one of the several motivations for the presented work in this chapter.

Model-based classification of normal and abnormal cases can immensely contribute to computer-aided diagnosis of EGMDs. Toward this end, a convenient mathematical model needs to be developed. Considering the fact that in reality there is no such thing as an ideal case of human/patient in terms of EGM data, such model has to be developed employing statistics (*e.g.* pulse amplitude) from a number of normal cases. Since esophageal contractions in a normal case consist of a set of periodic events [2], the model can be viewed as a dynamic periodic (or quasi-periodic) bio-system. Poincaré mapping (PM) [15][16], which recently emerged as a vehicle to the modeling of dynamic bio-systems based on their statistics, is considered.

In this chapter, brief overview of the background for the relevant techniques in pulse/spike detection and modeling is presented. Subsequently, the proposed techniques for detection/extraction and modeling of EGM data are described in detail. Furthermore, the proposed techniques are applied to the EGM data from 20 patients and the

experimental results are presented. Such results are compared to those from existing literature where applicable.

4.1 Overview of Pulse Detection Techniques

Pulse/spike detection is an important tool for segmentation of biomedical data, *e.g.* EGM signals. In this section, a quick overview of such techniques is presented. Techniques commonly used for measuring sharpness of waves are based on three-point interpolations, *e.g.* Taylor series approximation [17], which help estimate second derivative of a given signal. First derivative of a de-noised discrete signal $y(n)$ can be expressed as

$$y'(n) \approx (y(n) - y(n-1))/\delta, \tag{4.1}$$

where n and δ denote sample index and sampling period respectively. Second derivative of $y(n)$ can be expressed as

$$y''(n) \approx (y'(n+1) - y'(n))/\delta = (y(n+1) - 2y(n) + y(n-1))/\delta^2. \tag{4.2}$$

A major drawback of (4.2) is that it utilizes highly local data, *e.g.* a peak and its neighbours say, ignoring certain other points that also contribute to signal sharpness. In the literature, there exist some techniques, *e.g.* [18], which utilize "less local" data.

More recent techniques for pulse/spike detection utilize the time-frequency concept. A good example of such technique is the nonlinear energy operator (NLEO) proposed in [19]. NLEO is a simple way to measure the energy content of a discrete-time signal, based on an idea that energy variation of a signal indicates an event, *e.g.* pulse/spike. In [19], energy of a de-noised discrete signal $y(n)$ is defined as

$$E_{\text{Kaiser}}[y(n)] = y^2(n) - y(n-1)y(n-2). \tag{4.3}$$

In (4.3), E_{Kaiser} satisfies a key property, *i.e.*

$$E_{\text{Kaiser}}[A\cos(\omega_0 n + \theta)] = \frac{1}{2}A^2\omega_0{}^2. \tag{4.4}$$

From (4.4), the energy is proportional to both amplitude and frequency, and hence termed as frequency-weighted energy. In [20], NLEO was presented in a more general form using the energy definition

$$E_g[y(n)] = y(n-d)y(n-o) - y(n-q)y(n-r), \tag{4.5}$$

where $d+o=q+r$. In the cases where $d \neq o$ and $q \neq r$, E_g is more robust to "undesired artifacts", *e.g.* respiratory artifacts, owing to the absence of the squared term in (4.3).

Considering the above definition(s) of energy, the objective is to detect/track the energy changes in a given signal. Toward this end, in [20], a sliding temporal window is used, and the frequency-weighted energy of the first half of the window is subtracted from that of the second half, *i.e.*

$$S_{\text{NLEO}}(n_{\text{mid}}) = \left| \sum_{m=n_{\text{mid}}-L+1}^{n_{\text{mid}}} E_g(y(m)) - \sum_{m=n_{\text{mid}}+1}^{n_{\text{mid}}+L} E_g(y(m)) \right|, \tag{4.6}$$

where n_{mid} is the mid point of the sliding window of length $2L$, and m is the time-index. A major drawback of such techniques is that any change in the energy content of a biomedical signal results in a change in S_{NLEO}, regardless of the cause (*e.g.* undesired artifact). This drawback is critical in the case of EGM data as well, owing to the presence of artifacts. In this chapter, a new NPDT, which is relatively insensitive to artifacts, is proposed and applied to the EGM data.

4.2 Overview of Poincaré Mapping (PM)

In this section, PM [15], which is an emerging technique for modeling of periodic bio-systems, is reviewed. Given a bio-system with periodic (or quasi-periodic) dynamic behaviors, PM maps the "system behaviors" from a n-dimensional space onto a n-1

dimensional space referred to as the Poincaré section. Owing to this dimensional reduction, PM-based system analysis is often less complex. For instance, consider human body temperature measurements as a function of time that correspond to a two-dimensional dynamic system. If the temperature is observed to vary around 36°C, the system can be considered to possess quasi-periodic behavior. One way to apply PM to this scenario is to simply record the time points at which the temperature crosses the desired value.

Having quoted an example, the mathematics involved in PM technique is presented. Consider an autonomous differential equation in β given by

$$\frac{d\beta}{dt} = f(\beta), \quad f : R^n \to R^n, \quad \beta \in R^n, \tag{4.7}$$

and its solution/trajectory is of the form

$$\beta(t) = \phi(\beta_0, t_0, t), \tag{4.8}$$

where (β_0, t_0) is the initial condition. Let Γ represent an n-1 dimensional hyper-plane in the n-dimensional space, *i.e.*

$$\Gamma = \{\beta \in R^n \,|\, \varphi(\beta) = 0, \varphi : R^n \to R\}. \tag{4.9}$$

In this particular context, Γ is referred to as a Poincaré section. Poincaré map $\boldsymbol{g}$: $\Gamma \to \Gamma$ is defined as

$$\boldsymbol{g}(v_n) = \eta(\phi(\beta_n, t_n, t_n + T)), \tag{4.10}$$

where $v_n = \eta(\beta_n)$, $\beta_n \in \Gamma$, $\eta : R^n \to R^{n-1}$. In (4.10), T is the least time-interval, after which, the solution $\phi(\beta_0, t_0, t)$ starting from a point on Γ crosses Γ again. It is to be noted that each v_n is a n-1 dimensional point induced on Γ by the coordinate translation η from the n-dimensional space.

Conceptually, given a certain point on Γ, Poincaré map $\boldsymbol{g}$ provides the next point on Γ (*i.e.* after one time interval T). Figure 4.1 shows a conceptual illustration of a PM. PM has gained attention as a modeling technique with applications in biology and medicine [21]. Aside from advantages including simpler analysis and improved scope for visual assessment in terms of system complexity/nonlinearity, a major advantage is its relative insensitivity to artifacts [22]. Realizing the fact that EGM data typically contains natural artifacts, *e.g.* respiration artifacts, PM is applied for developing a computer-based model in order to classify EGM data patterns.

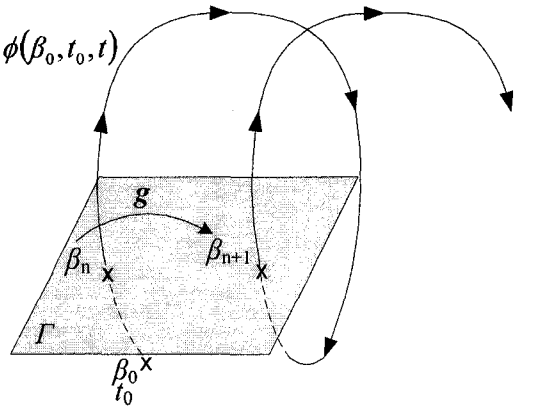

Figure 4.1 A conceptual illustration of Poincaré map g.

4.3 Proposed Nonlinear Pulse Detection Technique (NPDT)

In this section, a new EGM-oriented NPDT involving two phases described below is developed. It is to be noted that the raw EGM data is first de-noised using the WD overviewed in section 3.1.

4.3.1 Phase 1: Detection of Critical Points (CP)

The objective of the first phase is to locate the critical points in the de-noised EGM data fundamental to the patient's pulse shape. Conceptually, these points are the boundaries of the estimated straight lines fitted to the de-noised EGM data using a least square approach. In the case of an EGM pulse, a CP is either a pre-steep/rising point (p_r) or a post-steep/falling point (p_f).

In the proposed technique, the de-noised EGM data is first divided into a number of data segments based on the patient's pulse duration (typically 7-10s). Considering one such segment at a time, the technique involves sliding of what is referred to as a short-

time data analysis window, through the segment. The purpose of such window is to monitor the rate at which the EGM data trend changes within the segment. Detection of a number of consecutive rises (or falls) as the window slides in small steps indicates a CP. In terms of implementation, the length of the short-time analysis window and the number of consecutive rises (or falls) that ascertain a CP are determined according to the patient EGM pulse duration.

As mentioned earlier, considering a data segment at a time, the short-time window is slide with an objective to find a rising (or falling) trend. Within a window frame, least-square method is used to determine a straight line that approximates the data, with the slope of the line quantifying the rise (or fall). In other words, for a given set of data lying within the k^{th} short-time window, *i.e.* $y_k(w)$, $w = 1, 2, \ldots, W$, a line *i.e.* $l_k(w) = a_k w + b_k$, is determined, which best-fits the EGM data $y_k(w)$. This task is accomplished by minimizing the error function Π_k given by

$$\Pi_k = \sum_{w=1}^{W} [y_k(w) - l_k(w)]^2 , \tag{4.11}$$

where w is sample index, W is the short-time window length, and $y_k(w)$ and $l_k(w)$ are the de-noised and fitted data respectively. Solving $\frac{\partial \Pi_k}{\partial a_k} = 0$ and $\frac{\partial \Pi_k}{\partial b_k} = 0$ leads to computation of the unknown coefficients. For example, slope of $l_k(w)$ becomes

$$a_k = \frac{(W\sum_{w=1}^{W} y(w)l(w)) - (\sum_{w=1}^{W} y(w))(\sum_{w=1}^{W} l(w))}{(W\sum_{w=1}^{W} l^2(w)) - (\sum_{w=1}^{W} l(w))^2} \quad . \tag{4.12}$$

Condition $a_k > \xi$ is checked, where ξ represents the margin or threshold for a rising trend. If the condition is met, a similar process is performed on the k+1th short-time window to determine slope a_{k+1} and condition $a_{k+1} > \xi$ is then checked. Satisfaction of the latter condition indicates a rising trend and the first point in the k^{th} window, *i.e.* $y_k(1)$, is labelled as a CP. Similarly, the other CPs in the data segment are also detected. The above process is repeated for all the data segments of a patient's EGM data. In essence, at the end of phase 1, CPs in each data segment are detected. An illustrative example of the proposed technique in the case of a 15s long data segment is shown in Figure 4.2.

4.3.2 Phase 2: Wave-Shape Determination and Line-Fitting

Consider one data segment at a time. Starting with the CPs detected in the first phase, the objective of the second phase is to determine the underlying wave-shapes and accordingly fit the CPs with straight lines. Basically, the wave-shape is determined by the location of p_r and p_f in the data segment.

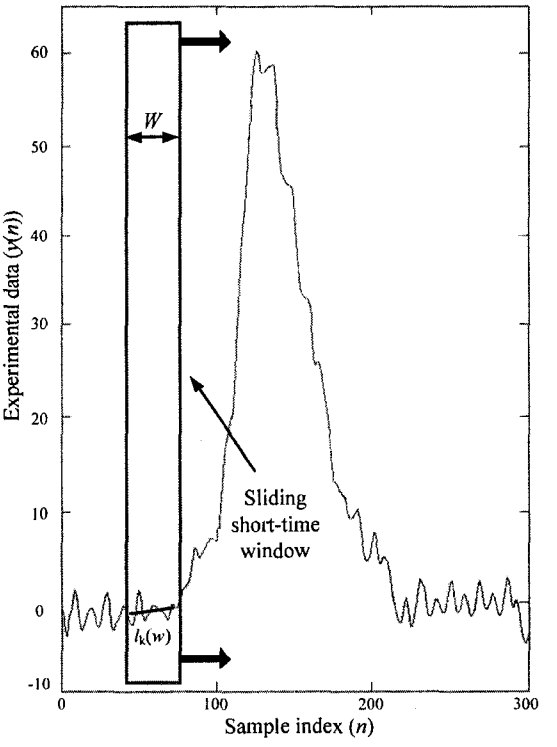

Figure 4.2. An illustration of proposed method for CP detection.

Specifically, in the case where p_r is detected prior to p_f (*i.e.* a rising data trend followed by a fall), a proper pulse (see Table 4.1) is deemed to be present in the data segment. In the case where p_f is detected prior to p_r, the data segment lies between two pulses. Since the length of the data segment is chosen such that there would not be two or more pulses within a segment, the possible scenarios for wave-shapes are limited to those presented in Table 4.1.

TABLE 4.1
POSSIBLE SCENARIOS FOR WAVE-SHAPES IN A DATA SEGMENT

Scenario	CP sequence	Wave-shape	Description
I	$p_r \rightarrow p_f$	_/_	Proper pulse
II	$p_f \rightarrow p_r$	_/	Between pulses
III	No CP	-----	No event

Once the wave-shape corresponding to a data segment is determined, the EGM data between the two CPs occurring at time instants n_p and n_{p-1} is estimated by a straight line, *i.e.* $e_p(n) = m_p n + u_p$, obtained using the least-square method. At the end of phase 2, critical information pertinent to the EGM data, *i.e.* EGM pulses, are detected and fitted with straight lines. The detected/extracted EGM signal, *i.e.*

$$e(n) = \begin{cases} e_1(n), & 1 < n \le n_1 \\ e_2(n), & n_1 < n \le n_2 \\ \vdots & \\ e_p(n), & n_{p-1} < n \le n_p \end{cases}, \tag{4.13}$$

where p denotes the CP index, formed by straight lines contains only those portions of the EGM data that are diagnostically important. An example of such a signal is depicted in Figure 4.3. In essence, the signal resulting from the proposed technique is suitable for computer-aided model-based classification into normal and abnormal cases. The flow-chart of the proposed NPDT is shown in Figure 4.4.

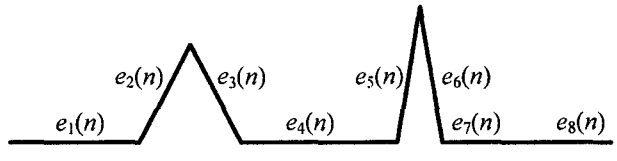

Figure 4.3 Extracted and linearly estimated EGM data by NPDT.

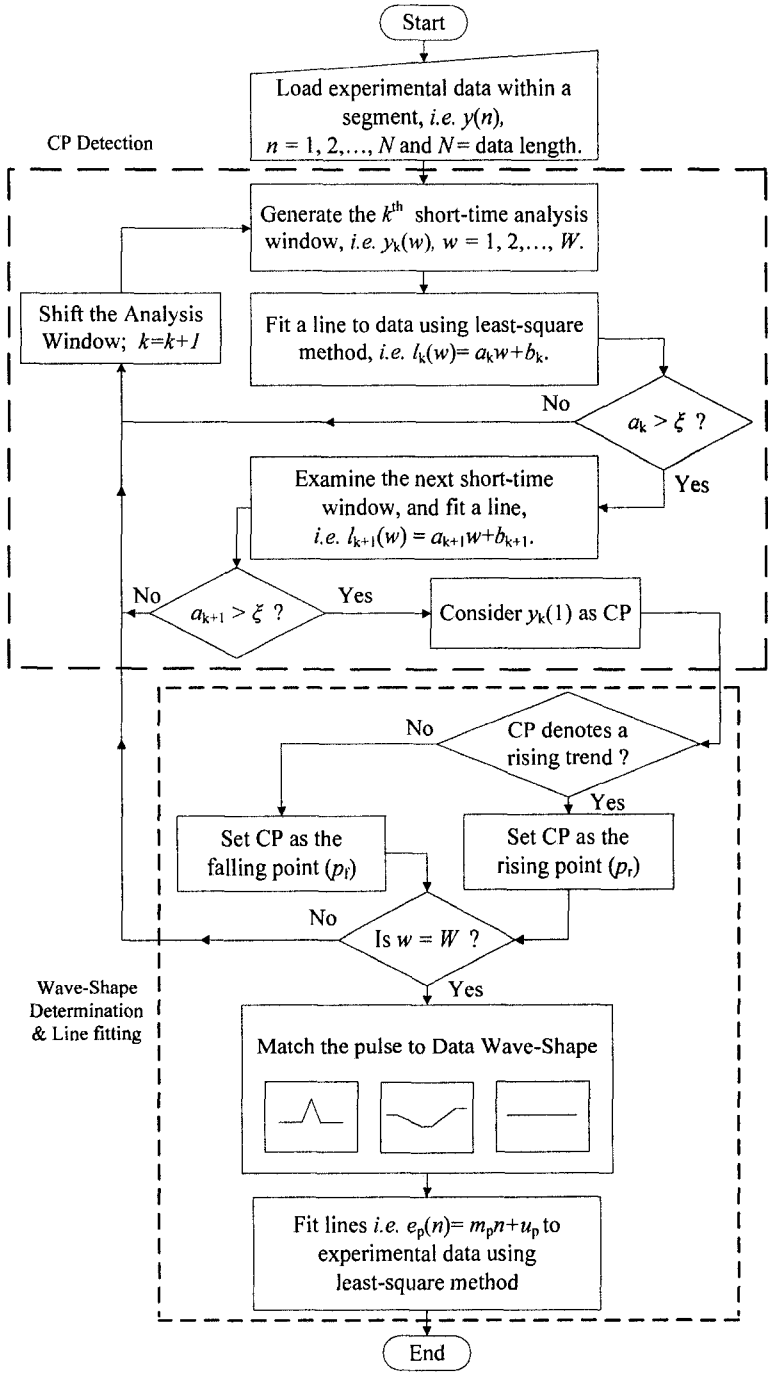

Figure 4.4 Overall Flowchart of the proposed NPDT.

4.4 Poincaré Map Based Pulse Modeling

PM reviewed in section 4.2 is applied to the modeling of EGM data. The proposed technique, which involves generation of a statistical model for classification of normal/abnormal cases, is described in this section.

As mentioned, there is no such thing as an ideal EGM pulse (or an ideal patient). In other words, even for normal cases, there exist different EGM pulse characteristics (*e.g.* amplitude, shape etc). Consequently, there is no definite scheme for classification into normal and abnormal cases. In such cases, development of a model based on pure mathematical formulae, is not preferable [21]. Black-box modeling techniques (*e.g.* artificial neural networks), although general, require excessive amounts of training data, *i.e.* widely varying patient data, and hence not efficient. As such, there is a need for techniques, which bring out statistical features from modest amounts of available biomedical or EGM data, in numerical/visual form. Motivated by this scenario PM has been used as a vehicle to statistical pulse modeling (SPM) of EGM data.

From the proposed NPDT, important information including the estimated slopes representing the EGM signal rise/fall and their order of occurrence are available. The objective of SPM is to model both the quantitative values of slopes (*i.e.* m_p) and their order of occurrence (*e.g.* a signal rise followed by a fall). Considering the detected/extracted EGM signal $e(n)$ of (4.13), which consists of straight lines, a data set M is defined as

$$M = \{m_p \in R \,|\, m_p = e'_p(n),\ p = 1, 2, ..., P-1\}, \tag{4.14}$$

where p is the CP index, n_p is the time instant corresponding to p^{th} CP, and P is the total number of CPs. As can be seen, M includes the numerical/quantitative values of slopes corresponding to each CP and can be deemed to emulate the dynamic system of (4.8). In order to represent the order of occurrence of the slopes, two Poincaré sections Γ_1 and Γ_2 are defined for any given consecutive slopes in M (*i.e.* p^{th} and p+1th slopes), *i.e.*

$$\Gamma_1 = \{m_p\}, \tag{4.15}$$

and

$$\Gamma_2 = \{m_{p+1}\}. \tag{4.16}$$

Γ_1 and Γ_2 when defined for each pair of consecutive slopes will correspondingly produce a number of ordered pairs of slopes, *i.e.* (m_p, m_{p+1}) that contain both the quantitative value of slopes as well as their order of occurrence.

An effective way to depict Poincaré sections Γ_1 and Γ_2 is to graph them using an orthogonal coordinate system. Such plots lead to effective visual representation of PM,

i.e. $\boldsymbol{g}$: $M \rightarrow M$. Once such graphical representation becomes available, given the current slope (say m_1), all the future slope values can be iteratively found using the graph. Since this concept is new in the context of EGM data, an illustrative explanation follows.

Consider the detected/extracted and line-fitted EGM data of Figure 4.3 employing the proposed NPDT. Applying the proposed PM technique (including generation of ordered pairs and representing them on a two dimensional m_p-m_{p+1} graph) leads to what is referred to as a Poincaré plot (Figure 4.5). Although simple, the plot conveys information with regard to slope values as well as correlation between consecutive slopes corresponding to the extracted EGM pulses. In other words, the plot offers information about any given EGM pulse, both in terms of its "shape characteristics" and its "location" in a stream of EGM pulses. As such, the plots facilitate observation of the dynamics of the EGM pulses in a given patient, by medical experts.

Interestingly, for a comprehensive set of EGM recordings (including a vast number of EGM pulses), the plot appears as a blur of points (see Figure 4.6). Based on the shape of the blur, one can fit a geometrical shape to the blur, mathematically characterize the shape, and extract key statistical information about the EGM pulses. An example illustrating this approach in the case of heart-rate variability measurements is presented in [23]. Following such an approach, a patient's EGM pulse stream can be statistically quantified (*e.g.* standard deviation, variance, etc) after fitted a suitable geometrical shape (*e.g.* circle). Such statistical information can be used as a basis for differentiation between normal and abnormal cases. As an example, consider the EGM

pulse stream of Figure 4.3 fitted to a circle. Standard deviation (SD) is denoted by the radius (R) of the circle, and variance (V) can be evaluated using

$$\mathrm{V} = \frac{A}{\pi}, \tag{4.17}$$

where A denotes area of the circle. From a diagnosis point of view, medical experts can define/specify a range for R, within which a patient is considered normal.

The proposed NPDT followed by the proposed SPM technique are applied to the EGM data of a number of patients, and the results are presented in the following section.

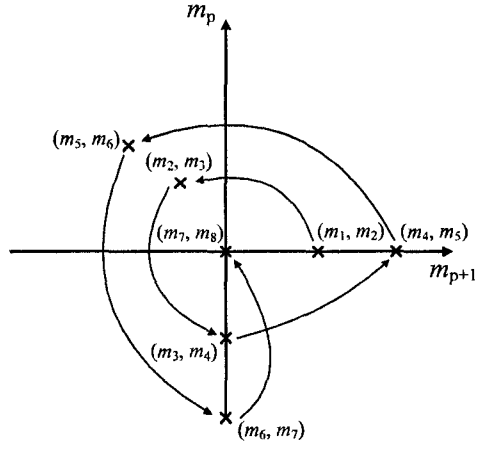

Figure 4.5 Poincaré plot of consecutive slopes using the proposed method.

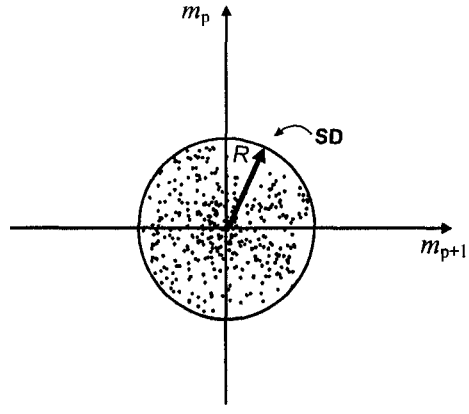

Figure 4.6 An example of a Poincaré plot illustrating the geometrical shape fitted to a blur of points.

4.5 Experimental Results

In this section, the experimental results of the proposed NPDT and SPM are illustrated. Both the techniques are applied to the real EGM data from patients and the results are shown. The presented EGM test results are obtained using the esophageal body examination procedure as part of the EGMDs diagnosis. The sampling rate in the experiments is chosen to be 16 Hz.

4.5.1 Experimental Results from NPDT

The proposed NPDT is applied to the de-noised EGM data of all 20 patients. The algorithm is implemented in the *MATLAB* environment.

A de-noised 10 minute EGM data recording of each patient (about 9600 data samples based on a sampling rate of 16 Hz) is considered. Each patient's data is divided into 40 segments of length 15s (240 samples), noting the patient's pulse duration, which

is typically 7-10s. Each of the segments is analyzed using a short-time sliding window of length 1s (*i.e.* $W = 16$). Typically, threshold ξ lies within [0, 0.2] range and varies for the de-noised EGM data of different patients. Considering this, the proposed NDPT is run several times, *i.e.* for different values of ξ, in order to find the optimal ξ for each patient. For each ξ, CPs of a data segment are detected by sliding the short-time window, *i.e.* k =1, 2, ..., 15. The de-noised EGM data between the CPs are fitted by straight lines. More specifically, in our work, ξ leading to the least error between the de-noised EGM data and the line-fitted waveform is treated as the optimal ξ for the patient under consideration. For the purpose of illustration, Figure 4.7 shows the line-fitted NDPT result for one of the 20 patients over a 30s time-frame.

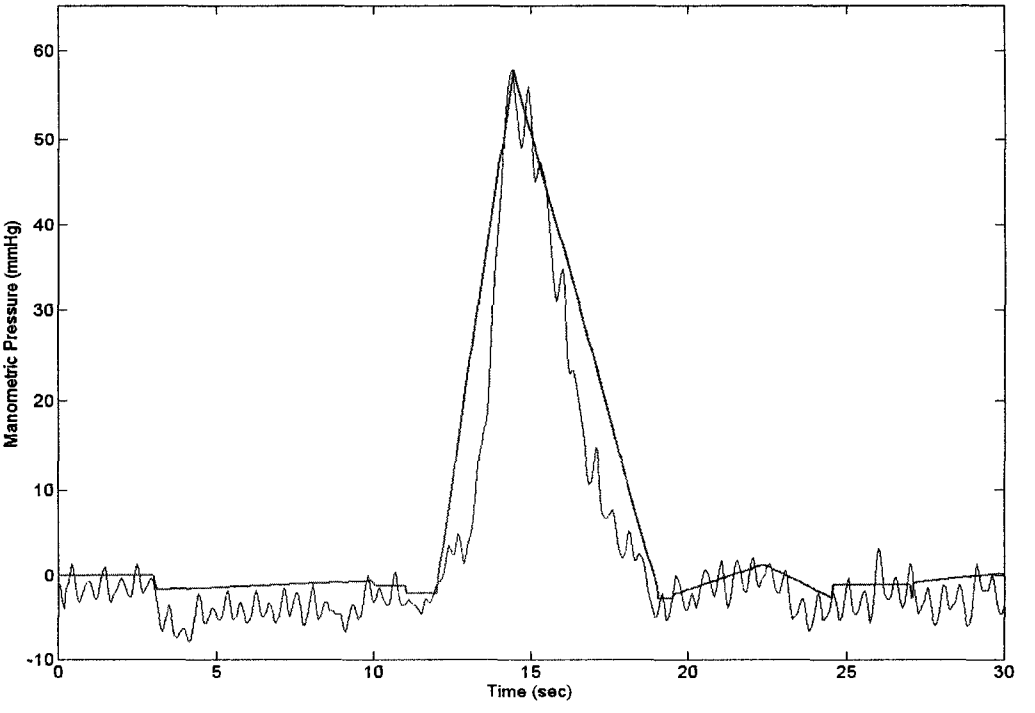

Figure 4.7 De-noised EGM signal and the fitted straight lines using NPDT.

The proposed NPDT is compared with existing techniques briefly mentioned/reviewed in section 4.1 (Table 4.2). Comparison is done in terms of accuracy, as quantified by normalized pulse duration error (*NPDE*), *i.e.*

$$NPDE = \frac{\sum \left| Detected \quad pulse \quad duration \quad - Actual \quad pulse \quad duration \right|}{\sum Data \quad segment \quad duration}, \quad (4.18)$$

in terms of efficiency, as quantified by accurate pulse detection rate (*APDR*), *i.e.*

$$APDR = \frac{\sum No.\ of \quad Accurate \quad pulses \quad detected}{\sum No.\ of \quad Total \quad pulses \quad detected}, \quad (4.19)$$

and in terms of sensitivity (ε), *i.e.*

$$\varepsilon = \frac{Minimum \quad detected \quad pulse \quad amplitude}{Average \quad pulse \quad amplitude}. \quad (4.20)$$

De-noised EGM data of all 20 patients is used. Table 4.2 shows that the proposed NPDT is both accurate and efficient compared to other techniques as indicated by the values of *NPDE* and *APDR* respectively. In addition, the proposed NPDT offers the best

sensitivity for detection of EGM pulses. However, it is worth-mentioning that the existing techniques used for comparison have been shown to be accurate/useful for detection/extraction of certain classes of biomedical signals such as EEG signals.

TABLE 4.2
COMPARISON OF SPIKE DETECTION TECHNIQUES

Detection Technique	***NPDE***	***APDR***	ε
Taylor Series 2nd Derivative [17]	0.7	0.13	0.61
Extrema based Estimation [18]	0.8	0.2	0.41
Least Square Acceleration [12]	0.4	0.83	0.35
Non-Linear Energy Operator [19]	0.6	0.78	0.56
Proposed NPDT	0.2	0.94	0.27

4.5.2 Experimental Results from SPM Technique

The proposed SPM technique, implemented in *MATLAB*, is applied to the detected/extracted and line-fitted EGM data of all 20 patients (10 normal cases and 10 abnormal cases). For brevity, SPM results of one normal case and one abnormal case are presented in this section.

For each patient, the ordered pairs of consecutive slopes from NPDT, *i.e.* (m_p, m_{p+1}), are depicted as a Poincaré plot, using an orthogonal coordinate system. These plots offer an interesting perspective to the review of EGM pulse dynamics. In order to bring out the differences between normal and abnormal cases, the adjacent points on these plots are connected using straight lines. The objective of such an exercise is to see if there

exists notable visual distinction between Poincaré plots of normal and abnormal cases. Poincaré plots consisting of 120 ordered pairs, *i.e.* $P = 120$, of a normal case and an abnormal case, with adjacent points connected, are shown in Figures 4.8 and 4.9 respectively.

A visual inspection of Figures 4.8 and 4.9 shows that the Poincaré plot of a normal case shows a regular pattern/trend, which is lacking in that of an abnormal case. In other words, given the current slope value in the case of a normal patient, there seems to be a possibility to find future slopes exploiting such pattern. This observation forms a "qualitative basis" for classification of normal and abnormal cases. Within the cases exhibiting regular patterns, certain abnormalities (*e.g.* out-of-range pulse amplitude) can not be ruled out. As such, a "quantitative approach" to further studying the Poincaré plots of probable normal cases is of interest.

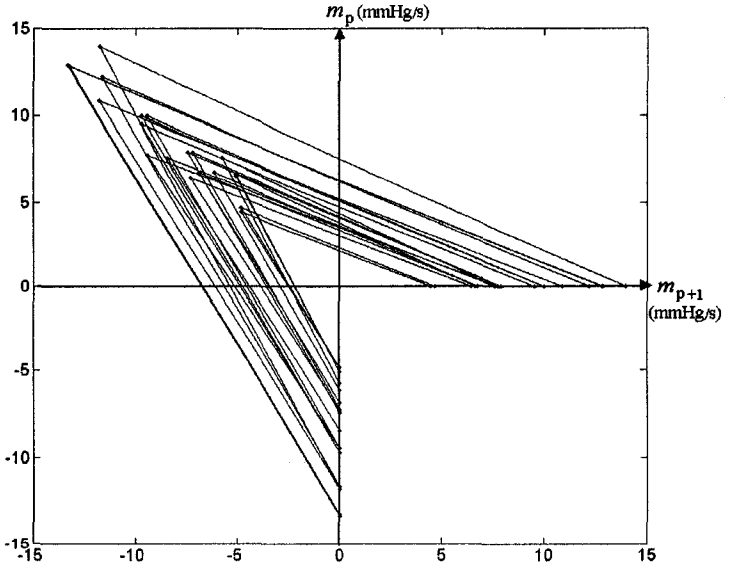

Figure 4.8 Poincaré plot of consecutive slopes for a normal case using SPM.

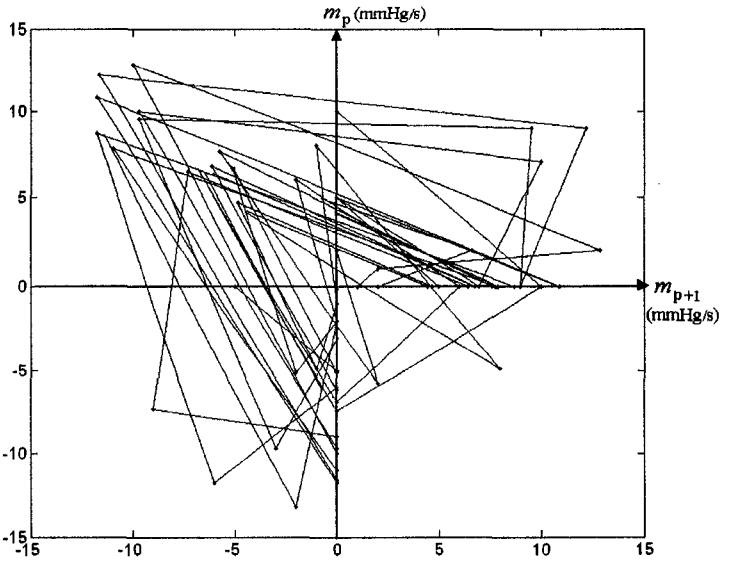

Figure 4.9 Poincaré plot of consecutive slopes for an abnormal case using SPM.

From the visual inspection of Poincaré plots of all 10 normal cases, it has been determined that an isosceles triangle best-fits the regular patterns. Figure 4.10 shows an example of one such fitted triangle along with its geometrical parameters, *i.e.* equal sides' length (a), non-equal side's length (b), and height (h). These parameters have a potential to offer key statistical information about each patient's data.

The next step is to relate the above-said triangle parameters to EGM pulse dynamics using mathematical equations. One of the diagnostically critical information with regard to a patient's EGM pulses is the maximum/minimum of pulse sharpness or slope. This information can be related to the height of the isosceles triangles, with the outer triangle height (h) and the inner triangle height (H) representing the maximum and minimum respectively, as seen in Figure 4.11. Maximum sharpness indicator (MASI) is defined as

$$h = \sqrt{a^2 - \frac{1}{4}b^2}\,, \tag{4.21}$$

and minimum sharpness indicator (MISI) is defined as

$$H = \sqrt{A^2 - \frac{1}{4}B^2}\,. \tag{4.22}$$

Symmetry of the patient EGM pulses also offers diagnostically important information. The patient's pulse symmetry index (PSI) using parameters σ_1 and σ_2 (of Figures 4.10 and 4.11) is defined as

$$\text{PSI} = \begin{cases} \dfrac{\sigma_2}{\sigma_1}; & \sigma_1 > \sigma_2 \\ \dfrac{\sigma_1}{\sigma_2}; & \sigma_2 > \sigma_1 \end{cases}. \tag{4.23}$$

Ideally, the value of PSI regarding to an EGM data including a number of symmetrical pulses is 1.

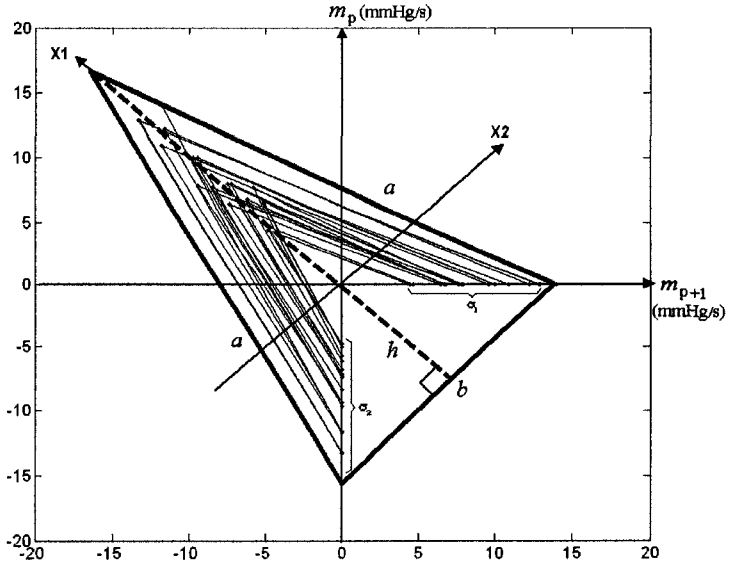

Figure 4.10 Isosceles triangle fitted to Poincaré plot of consecutive slopes for a normal case.

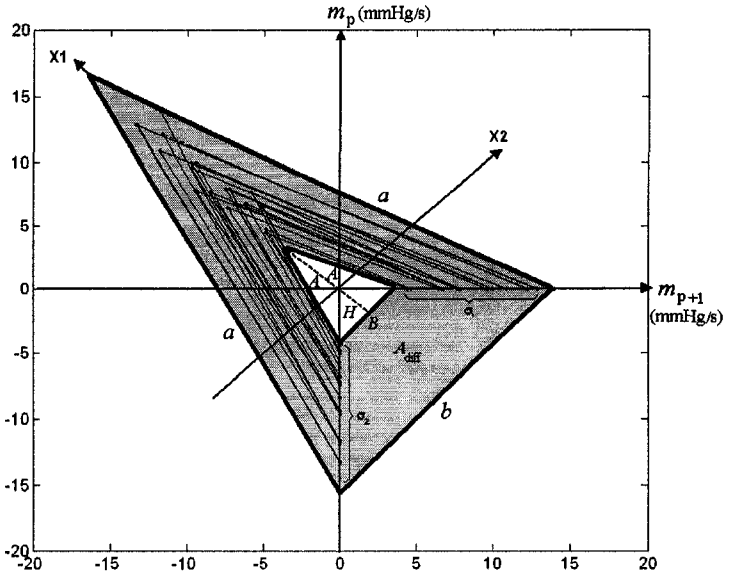

Figure 4.11 Realization of A_{diff} from Poincaré plot for a normal case.

A yet another interesting information with regard to patient's EGM pulses comes from the standard deviation (SD) of slopes. For quantifying this measure, area A_{diff} is defined as

$$A_{\text{diff}} = A_{\text{out}} - A_{\text{in}} = \frac{1}{2}(b.h - B.H)\,. \tag{4.24}$$

Substituting for h from (4.21), and H from (4.22), we have

$$\text{SD} \propto A_{\text{diff}} = \frac{1}{2}\sqrt{a^2b^2 - A^2B^2 - \frac{1}{4}(b^2 - B^2)}\,, \tag{4.25}$$

which is an indicator for the consistency of a patient's EGM pulses.

The proposed SPM technique (including all the above measures) is applied to the EGM data of 10 normal patients, and the numerical results are summarized in Table 4.3. Such results convey key statistical information regarding to patients' EGM pulses as describe by the measures. A range can be specified by experts for the numerical results regarding each measure in which the patient is considered as normal. Interestingly, meaningful data is not only obtained through the particular measures cited in Table 4.3, but the combination of measures has enabled the observation of correlation between them. For instance, in cases where the MASI and MISI are relatively high yet within a

normal range, the higher values of SD are considered normal. Therefore, the range for the SD values in which the patient is considered as normal is dictated using MASI and MISI. Such a quantitative approach to the study of Poincaré plots provides an effective tool for further assessment of EGM pulses aiming at differentiating certain abnormalities.

TABLE 4.3
STATISTICAL MEASURES FOR EGM PULSES REALIZED BY SPM FOR 10 NORMAL PATIENTS

Patient	MASI (mmHg)	MISI (mmHg)	PSI	A_{diff} $(mmHg)^2$
1	24	11	0.98	295
2	16	9	0.64	120
3	23	13	0.52	238
4	19	8	0.23	170
5	27	16	0. 82	343
6	37	26	0.69	282
7	25	11	0.71	310
8	22	12	0.42	225
9	29	16	0.43	364
10	14	9	0.71	114

4.6 Summary

In this chapter, new techniques to analysis and modeling of EGM data for EGMDs diagnosis are described. Subsequent to high-frequency noise filtering from EGM data, the proposed techniques include detection/extraction of diagnostically valuable portions of the EGM recordings, and development of a statistical model for differentiation between normal and abnormal cases. The raw EGM data from 20 patients is first filtered using the WD described in chapter 3. A new NPDT is developed to identify and extract the critical information, *i.e.* EGM pulses with emphasis on accuracy and efficiency. For comparison, the proposed NPDT and the similar techniques in existing literature are applied to the de-noised EGM data. Such comparison shows that the NPDT leads to better results in terms of accuracy. The detected/extracted EGM pulses are then used to generate a statistical model exploiting PM that classifies/differentiates normal and abnormal cases. Such model aids the medical experts in the EGMDs diagnosis based on EGM data.

Chapter 5

A New Approach for Treatment of Gastroesophageal Reflux Disease (GERD)

As mentioned earlier, GERD is the most prevalent EGMD-based disease that despite the numerous existing techniques for its treatment, research towards an effective cure has continued unabated. In this chapter, a novel idea for treatment of GERD using an electronic implantable device is described. Furthermore, a number of sample circuits for the proposed implant structure from the existing literature are presented.

5.1 A Potential Approach to GERD Treatment

As explained in section 2.8.2, acid reflux can occur during different mechanisms which may result in GERD. However, the common feature in all GERD cases is the LES failure to stay contracted in absence of a swallow. As such, a general solution for GERD treatment should involve the control of LES in order to assure its contraction at appropriate times. In the following, an engineering approach based on electrical stimulation of LES using neurostimulation techniques for GERD treatment is proposed.

5.1.1 LES Control Utilizing Neurostimulation Techniques

LES consists of a muscle that controls the transition of material at the junction between the stomach and the esophagus. Importantly, this muscle can be stimulated through its motor nerves/neurons using available neuroengineering techniques [24]. A good example for application of such techniques is presented in [25]. Ultimately, the control of LES can be accomplished by means of these techniques and it can be considered as an effective GERD treatment. In the next section, a new approach to implement this idea is described.

5.1.2 An Effective Approach to Realizing Neurostimulation-Based Control of LES

The control of LES using neurostimulation techniques can be implemented by using an electronic device implantable in the body of the patient. Such an implant is responsible to control the LES and guarantee the LES contraction and relaxation at appropriate times. Obviously, the implant device has to be supplied with electrical power

to be able to perform the control tasks. This power can be supplied by means of wireless power transmission methods dedicated to biomedical applications [25]. It should be noted that, the implant consists of a number of circuits/modules that have to be designed according to strict criteria such as low power consumption, low supply voltage, minimal chip area, etc. Therefore, analog circuit design techniques are required to achieve the desired criteria for circuits of the device. A number of sample analog circuits from the existing literature are presented in the following sections.

5.2 A Smart Implant Dedicated to GERD Treatment

In this section, the concept of the proposed implant device for GERD treatment is described extensively. The main idea of LES control through neurostimulation techniques is explained and the potential challenges/concerns are mentioned. The objective is to create a basis for further research regarding this subject.

5.2.1 LES Stimulation Concept

As explained in section 2.8.1, LES is a muscle that receives its control signals from parts of the brain through Vagus nerve. Therefore the control of LES can be accomplished through electrical neurostimulaion of the motor neurons included in the Vagus nerve. This stimulation can be done by applying low amounts of electric current (in the order of mAs), by means of simulation electrodes (*e.g.* cuff electrodes) [24].

There are two motor neuron groups included in the Vagus nerve, one producing contraction and the other relaxation of the LES. In other words, contractions and relaxations of the LES are two separate events that are produced by the brain and

transmitted by neurons. Therefore, the LES control procedure used by the proposed implant should include two separate sections dedicated for creation of contractions and relaxations. In the following section, the main tasks/responsibilities of the implant are described. Consequently, a control algorithm is developed based on these tasks/responsibilities.

5.2.2 Main Tasks/Responsibilities of the Implant

As explained in section 2.8.2, the main mechanism of reflux leading to GERD is the frequent TLESRs. In other words the high incidence rate of these transient LES relaxations leads to GERD overtime. Therefore an effective strategy to cure GERD is to reduce the number of TLESRs. As such, the tasks/responsibilities of the implant are determined so that the LES is forced to stay contracted at appropriate time thus reducing the TLESRs. It should be noted that the TLESR is a natural mechanism and occurs due to a number of reasons such as stomach distention caused by food or gas (which results in belching), excess body fat and stress. Consequently, the total elimination of all the TLESRs is not an option. However, the idea of reducing the number of TLESRs seems to be an effective means to cure GERD.

As explained, the implant is responsible to stimulate the LES to stay contracted unless there is a swallow event or a stomach distention. As such, there is a need for different sensors in order to detect swallows or stomach distentions. Based on the facts mentioned above, the main tasks of the implant are summarized as:

i) Detection of swallow events.

ii) Detection of stomach distentions.

iii) Contraction of the LES unless there is a swallow or a stomach distention.

iv) Relaxation of the LES when there is a swallow or a stomach distention.

It is to note that the contraction and relaxation of LES are two separate tasks ever since each of them is accomplished by stimulation of a different nerve group. An implant capable of realizing the above tasks has to be equipped with multiple channels of sensors and stimulators. In the following section a general scheme for implementation of the proposed implant system is described. In addition, a number of sample circuits proposed in the literature are also presented.

5.3 Implant System Structure and Circuits

The proposed implant system consists of two main units, one implanted in patient's body and another one being outside the body (see Figure 5.1). The first unit is the actual implant device which is responsible for the LES control. The second unit is the external controller unit which is responsible for transmitting electrical power and control commands to the implant unit. More precisely, it supplies the power for the implant and adds user-based control features to the system. The above mentioned units communicate through a wireless link for transmission of power and data. A suitable option for implementation of such a link is via inductive link using two coils, one on each unit.

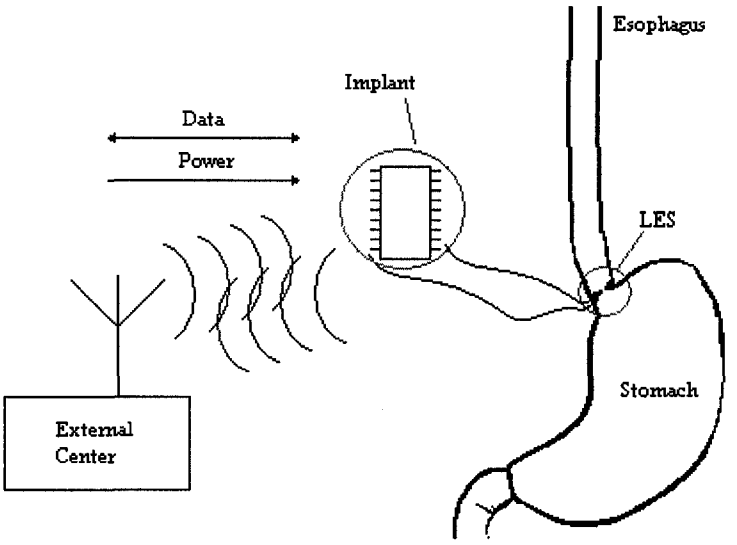

Figure 5.1 Proposed implant system.

The implant unit is determined to be in close contact with the target tissue in order to acquire the sensory signals and to stimulate the tissue. As such, this unit includes a control/logic module to manage the operation of the other modules in the implant and generate necessary control signals. The power needed for all the modules in implant unit is provided by a power recovery circuitry which receives the transmitted power from the external source. A communication circuitry is designed to receive the data which is mainly the user-implied control signals in emergency situations. A sensing module is determined to collect the desired physical quantity (*i.e.* displacement in this case) from the body tissue and provide such information to the control/logic unit. Stimulation of the target tissue is performed via the stimulator module which is designed to generate the suitable electrical signal for the specific tissue.

The external controller is responsible for transmission of power and user commands to the implant device. Therefore, it consists of a control/logic module to manage the control commands and a communication module for transmission of power and data. Figure 5.2 illustrates the different modules in the proposed implant structure. In the following sections a number of sample circuits for implementation of the proposed system are presented.

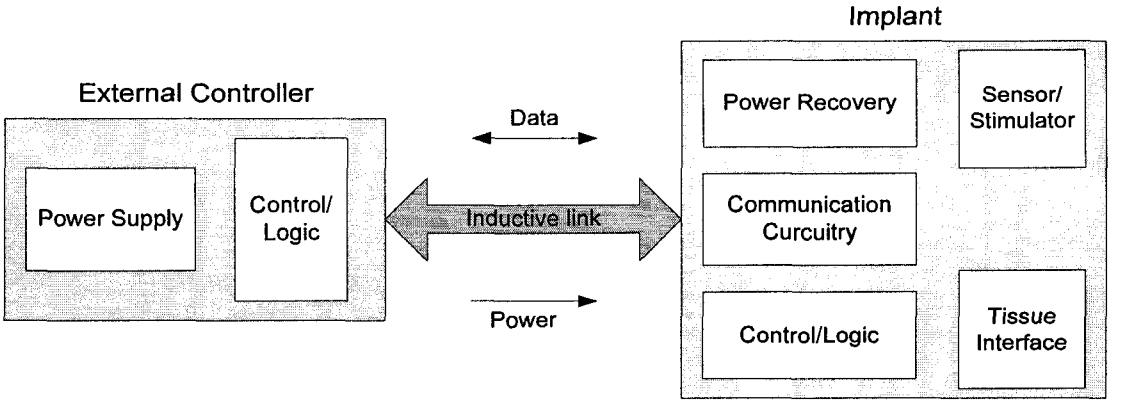

Figure 5.2 Implant structure.

5.3.1 The Power Recovery System

In this subsection a power recovery system to be implemented on the implant device is presented. Typically, the circuits designed for devices dedicated to nerve stimulation applications need a certain amount of stimulating current which requires a large voltage supply to drive the electrodes. This is due to the fact that the equivalent tissue impedance is in the range of several tens of kilo-Ohms and need significant amount

of power for stimulation. However, such devices normally contain a number of analog/digital circuitry (*e.g.* control/logic circuitry) that are designed to operate using low voltage supplies, in order to minimize the overall power consumption. Therefore, at least two level supply voltages are desired in such applications. The proposed integrated power recovery system is shown in Figure 5.3 [26]. The system is capable of providing dual regulated output voltages *i.e.* V_{High}, V_{Low}, to the stimulator output stages and other circuitry respectively.

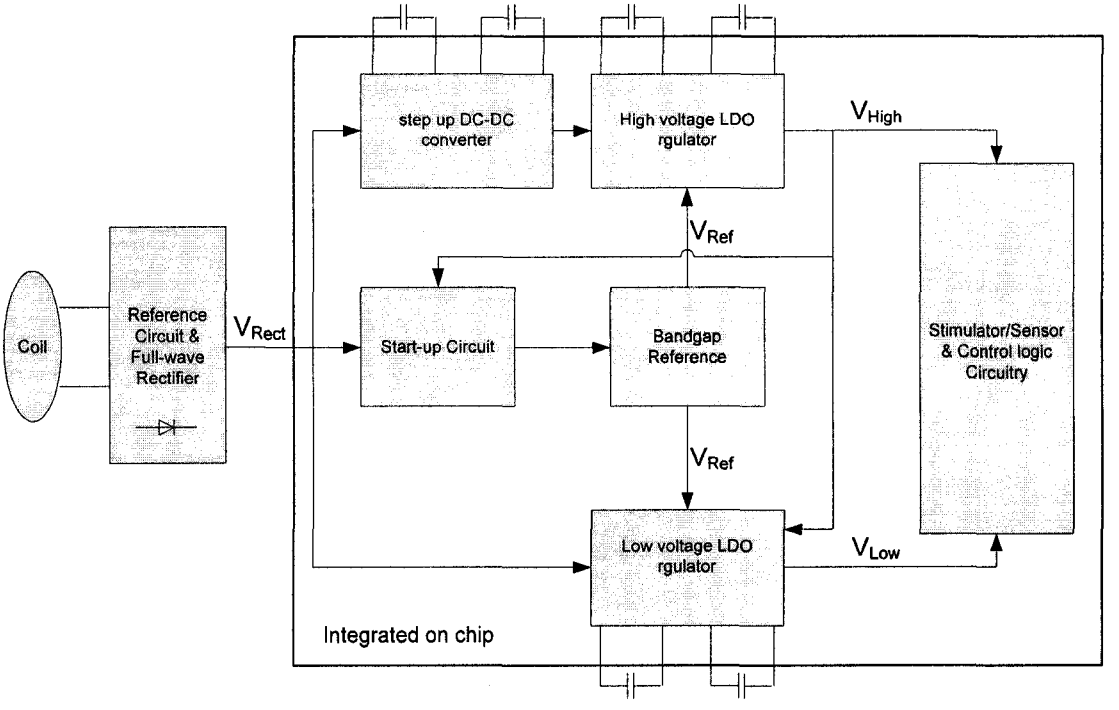

Figure 5.3 Power recovery system [26].

5.3.1.1 CMOS Full-wave Bridge Rectifier

The wirelessly transmitted power signal that is received through the coil/antenna of the implant device is rectified using a bridge rectifier (see Figure 5.3) and fed to the

other stages of the power recovery system. An applicable sample of a CMOS full-wave bridge rectifier is proposed in [27] (see Figure 5.4). Employing a full-wave bridge rectifier as compared to a half-wave rectifier significantly reduces the implant size and also helps the regulator to achieve better AC-DC conversion efficiency. In the circuit of Figure 5.4, diode connected pMOS transistors M_{P1} and M_{P2} and the diode connected nMOS transistors M_{n1} and M_{n2}, form a bridge for the received signal from the coil. Transistors M_{p3} through M_{p6} are auxiliary transistors which facilitate the function of M_{P1} and M_{P2}. Transistors Q_1 and Q_2 help the transistors M_{n1} and M_{n2} to return current from grounded substrate to the coil.

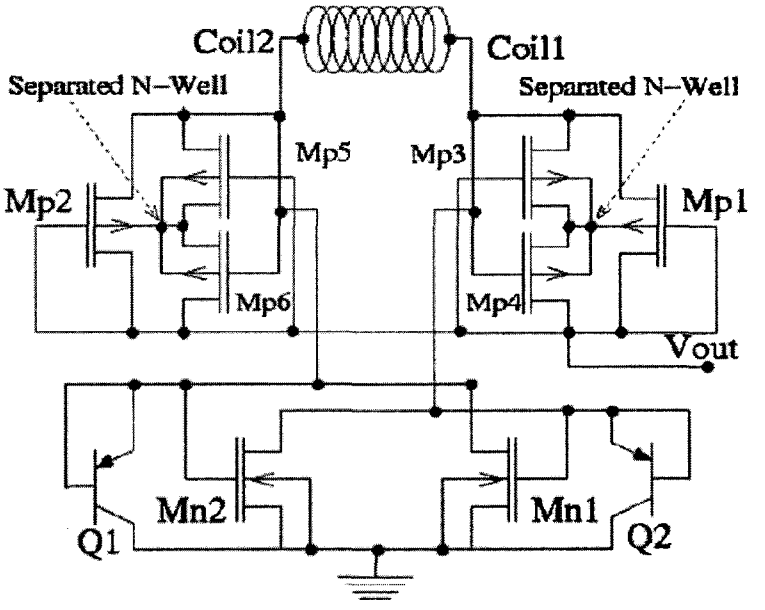

Figure 5.4 Integrated CMOS full-wave bridge rectifier [27].

5.3.1.2 Dual-Output Low-Dropout Voltage Regulator

As mentioned earlier, the wirelessly received energy must be rectified and regulated. This regulation can be achieved by using the regulator structure proposed in [26] known as low-drop-out (LDO) linear voltage regulator (see Figure 5.5). Typically, linear regulator consists of a voltage reference, a pass device, an error amplifier, and a resistive feedback network. It is mainly divided into two categories according to the pass transistor device: p-type and n-type regulators. Each has its own advantages and drawbacks. The latter structure is often preferred due to its less stability problems, better line load regulation, and naturally low-ohmic output impedance structure. However, the conventional nMOS regulator suffers from large dropout voltage problem, due to the fact that the gate potential voltage of the pass transistor needs at least one threshold voltage (V_{th}), higher than the regulated output. The problem can be mitigated by using a native transistor (*i.e.* NM_1 in Figure 5.5), available in many modern CMOS processes. The difference between a native CMOS and a usual CMOS is that a native CMOS is a transistor which skips the step of adjusting the threshold-voltage (V_{th}) during its fabrication process. Regulators using n-type pass devices show fewer stability problems, better regulation and lower output impedance characteristics compared to their p-type counterparts.

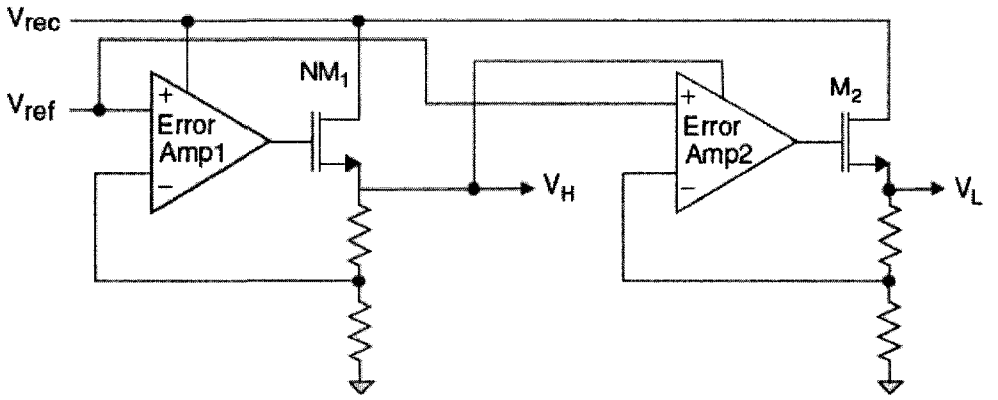

Figure 5.5 A typical dual output (LDO) voltage regulator from [26].

5.3.1.3 CMOS Bandgap Reference

A bandgap reference circuit is desired to provide a reference voltage to both regulators in the system. A sample CMOS bandgap reference circuit is described in [26]. Unlike in most conventional bandgap reference applications, the requirement of temperature dependency for the circuit is relaxed. This is due to the fact that the circuit environment temperature (*i.e.* patient's body temperature) in the target application is not widely varied.

5.3.1.4 Start up Circuit

According to the fact that both the voltage regulator and the bandgap reference in the power recovery module are interdependent, meaning they need each other to function properly, a start up circuit is used to provide the bandgap reference with the rectified voltage on power up, and then switch to the regulated voltage when it becomes available.

The start-up circuit compares V_{rec} and V_{High}, and feeds the larger of the two to the bandgap reference. The schematic of the start up circuit is shown in Figure 5.6 [26].

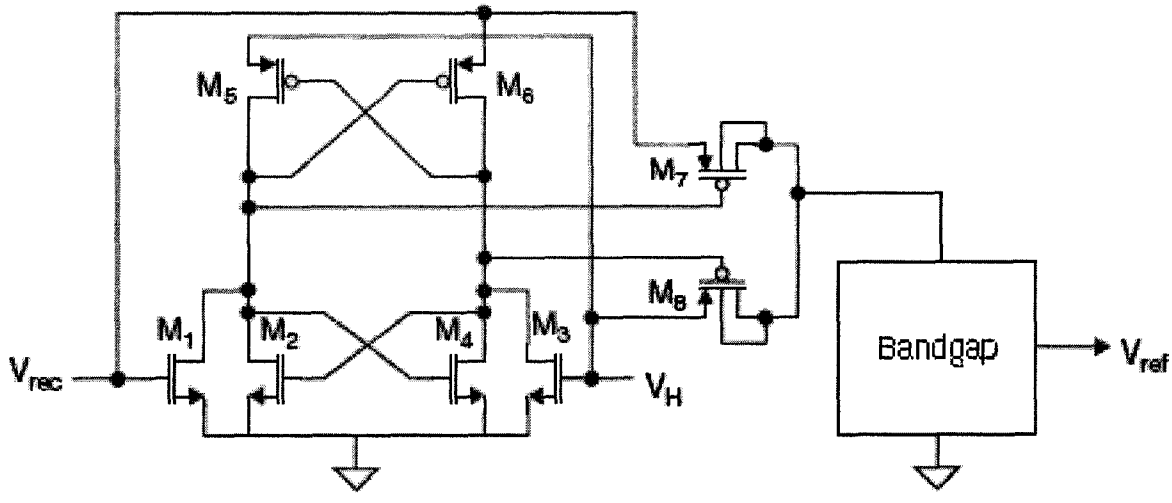

Figure 5.6 Start up Circuit [26].

5.3.1.5 DC-DC Converter

A DC-DC converter (level shifter) [27] can be used to supply and generate the desired voltages V_{Low} and V_{High} to the regulators. A typical circuit for the level shifter is shown in Figure 5.7. The output voltage is simply equal to input voltage minus two gate-source voltages *i.e.* $V_{out} = V_{in}-(V_{SG1}+V_{SG2})$. The circuit consumes very low power which is a significant advantage for the target application.

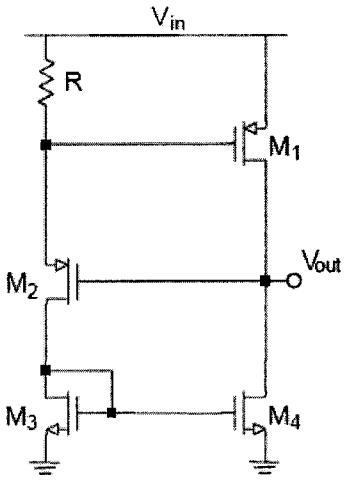

Figure 5.7 Level shifter circuit [27].

5.3.2 Communication System

In this section, the desired building blocks of the communication system are introduced and in each case a sample circuitry is proposed. As described earlier, there is an external controller in the proposed implant system which is responsible for transmission of power and user commands to the implanted device via an inductive link. The inductive link between the two units is a bi-directional data link and is composed of two separate links for data transmission. The first link transmits the data from the external controller to the implanted device (*i.e.* downlink) and the second link transmits the data from the implanted device to the external controller (*i.e.* uplink). These links can be implemented using different circuit strategies aiming to meet a number of certain criteria (*e.g.* data transmission rate, power consumption, etc.) in different applications. In fact, bi-directional data transmission has become a trend in state-of-the-art design of wireless biomedical systems. Recently, a few wireless inductive link designs have been

reported. The main data communication characteristics of these works are summarized in Table 5.1.

TABLE 5.1 RECENT DATA COMMUNICATION TECHNIQUES PROPOSED FOR IMPLANTABLE DEVICES

References	Downlink (rate)	Uplink (rate)	Carrier (Hz)	Power Consumption	Technology
[28]	Packet detection	Burst of RF energy	2.5 M	-	2 μm CMOS
[29]	PWM-ASK (250 kbps)	ASK	1~10 M	5 mW	1.2 μm CMOS
[30]	ASK	PWM-ASK (125 kbps)	4 M	10–90 mW	3 μm BiCMOS
[31]	ASK (120 k)	BPSK (117–234 k)	10 M	4.5 mA	2.5 μm BiC
[32]	OOK (100 kbps)	No	5 M	0.5 mA, 10 V	2 μm CMOS
[33]	OOK	LSK (200kbps)	6.78 M	<120 mW	1.2 μm CMOS
[34]	BPSK	BPSK	13.56 M	652 μW	0.18 μm CMOS

In this work the proposed link for the communication in implant system is known as binary phase shift keying (BPSK) [34]. BPSK is a process where the target binary signal shifts the phase of a carrier waveform between 0° and 180°. This is equivalent to multiplying the carrier with a bit stream of '1' and '−1' representing high and low states respectively. As such, a BPSK modulator simply multiplies a target signal *i.e.* $m(t)$ to a carrier *i.e.* $\sin(\omega_1 t + \theta_1)$. However the demodulation process is not as simple. Figure 5.8

illustrates the block diagram of the BPSK demodulator including a structure known as Costas loop. A brief description of the demodulator function follows.

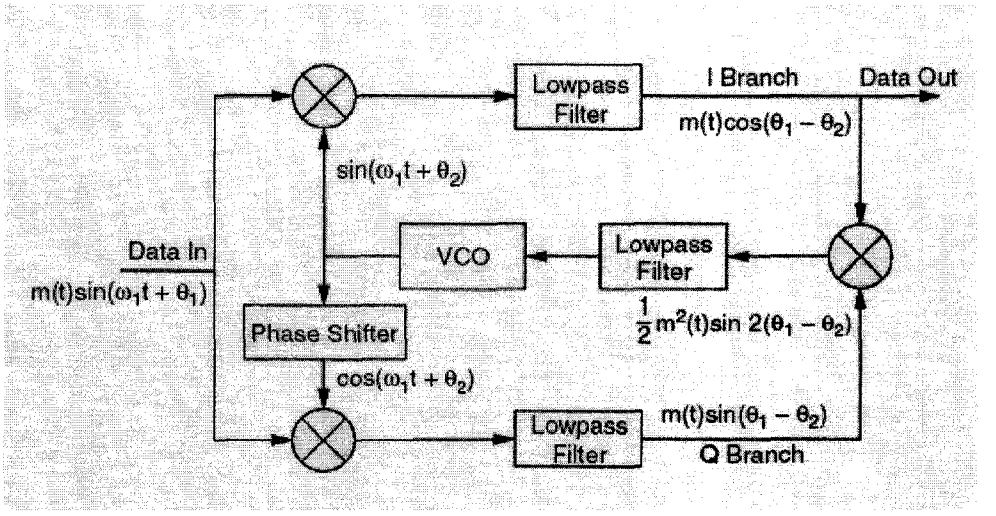

(a)

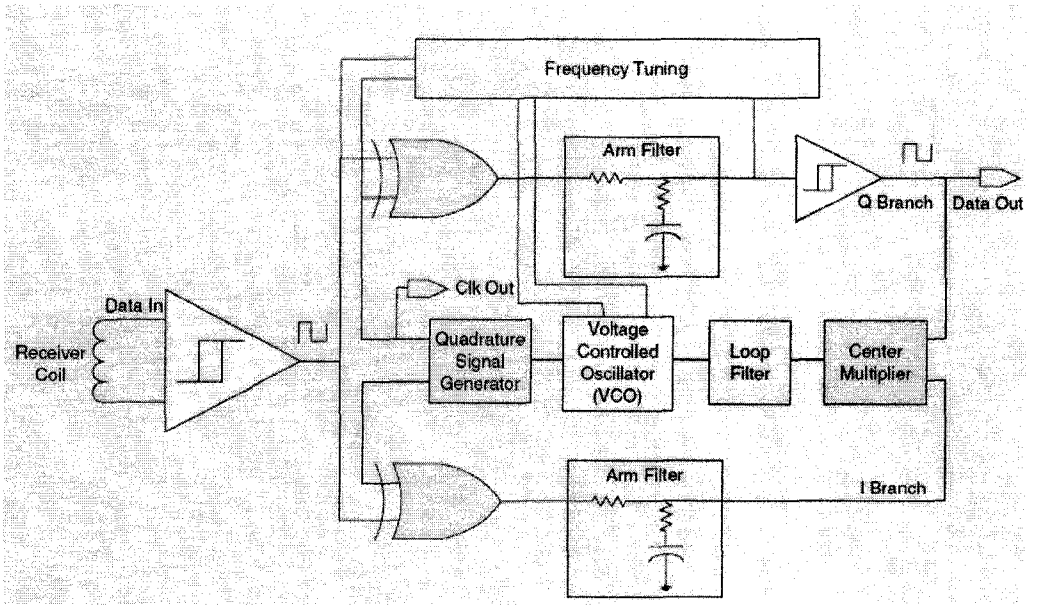

(b)

Figure 5.8 Inductive link for transmitted data: (a) Costas loop demodulator (b) detailed demodulator block diagram [35].

The input signal of the demodulator is the product of a data stream and a carrier. Here, the purpose is to obtain the data stream by separating it from the carrier signal. Assume that in Figure 5.8(a), the term $m(t)$ represents the data stream in the input signal composed of either '1' or '−1' and the term $\sin(\omega_1 t + \theta_1)$ is the carrier. After passing through the low-pass filters, the outputs of the upper and lower branches are expressed as $V_{OI}(t) = m(t)\cos(\theta_1 - \theta_2)$ and $V_{OQ}(t) = m(t)\sin(\theta_1 - \theta_2)$. By means of an additional multiplier and a loop filter at the center branch, the control voltage of the VCO becomes only proportional to the phase difference $(\theta_1 - \theta_2)$. In case there is no phase difference in that signal the required demodulated signal is achieved in the output. In other words, the system tries to make the phase difference $(\theta_1 - \theta_2)$ equal to zero by finding the phase θ_2 equal to θ_1. Consequently, the target signal $m(t)$ is obtained from the upper branch in Figure 5.8(a).

The detailed block diagram of the Costas loop demodulator is shown in Figure 5.8(b) The multipliers are implemented using simple XOR gates and the low pass filters are RC low-pass filters. These low-pass filters are necessary in order to cancel any unwanted harmonics since the multiplication is a nonlinear process. In the following subsections a number of sample circuits for the demodulator building blocks are described.

5.3.2.1 Comparator

In the detailed diagram of Figure 5.8(b), there are two comparators located at the input and upper branch. The first comparator converts the input signal to the square

waveform. This allows using simple digital phase detectors in the circuit. The second comparator assures that the output signal is in the form of a data stream of '1s' and '−1s'.

The comparator circuit is shown in Figure 5.9 [35]. The whole circuit consists of two parts. On part provides the reference voltages for the bias of the circuit and the other part is the high gain differential amplifier which does the comparison of the input signals. The reference voltage circuit is shown on the left side of the Figure 5.9. The nMOS transistors, M_1 and M_2, are the differential input pair and form the main core of the comparator. Transistors M_3 and M_4, are current sinks to supply the required current for the differential pair. Transistors M_5 - M_{12}, are current mirrors as active loads for the differential pair to boost its gain. The output stage consists of transistors, M_{13} - M_{18}, and M_{19} - M_{24}. Two digital buffers are also put at the output for the isolation of the circuits. The employment of two current mirror transistors, M_{17} and M_{23}, eliminated the need of a common mode feedback circuit (CMFB), which has simplified the overall system.

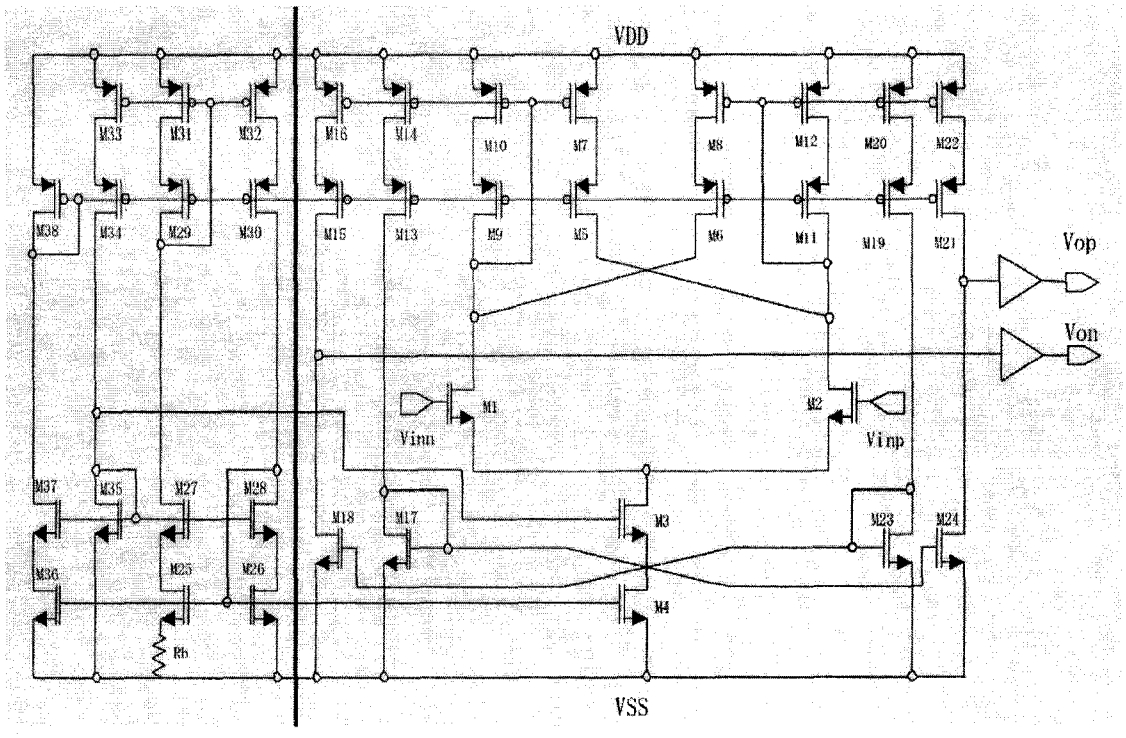

Figure 5.9 Comparator for the demodulator [35].

5.3.2.2 Phase Detector and Multiplier

The phase detector and multiplier circuit is shown in Figure 5.10 [35]. As the input carrier and the output of upper branch have been converted into the binary form, a fully differential exclusive OR is used as the center multiplier. This can be simply implemented by means of transmission gates shown in Figure 5.10. These multipliers can be simple AND gates implemented by CMOS technology.

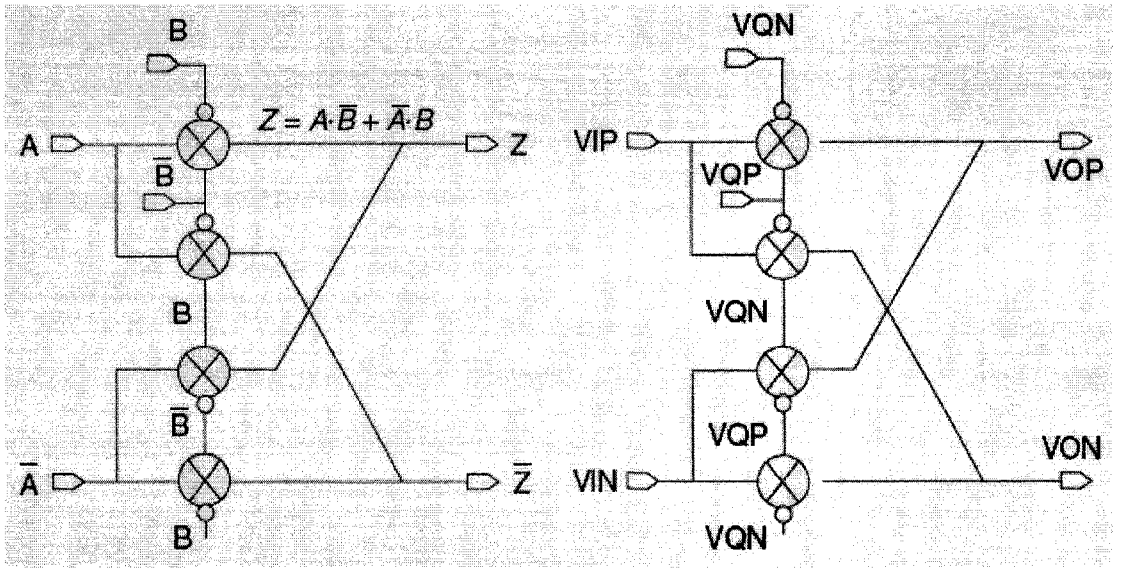

Figure 5.10 Phase detector and multiplier circuit [35].

5.3.2.3 Voltage Controlled Oscillator (VCO)

The structure of the voltage controlled oscillator for the demodulator is shown in Figure 5.11. The whole structure is made of two parts: a transconductance cell (left side) and oscillation cell (right side). The transconductance cell is designed to convert the applied input voltage to a control current effective to the oscillation frequency of the VCO. The oscillation cell is the core of the VCO which generates the oscillation frequency. Transistors (M_1, M_2) operate as switches, which are turned on/off in turn in accordance with voltage potentials of their gate and source terminals. The frequency is controlled by a linear transconductance cell which generates a control current injected to the oscillation cell in Figure 5.11. This control current is proportional to the applied input voltage of the VCO. The oscillation is generated by turning on/off the transistors M_1 and

M_2 resulting charge/recharge of the capacitor C_1. Any change in the control current is copied to the charging current of the capacitor thus results in the frequency of oscillation.

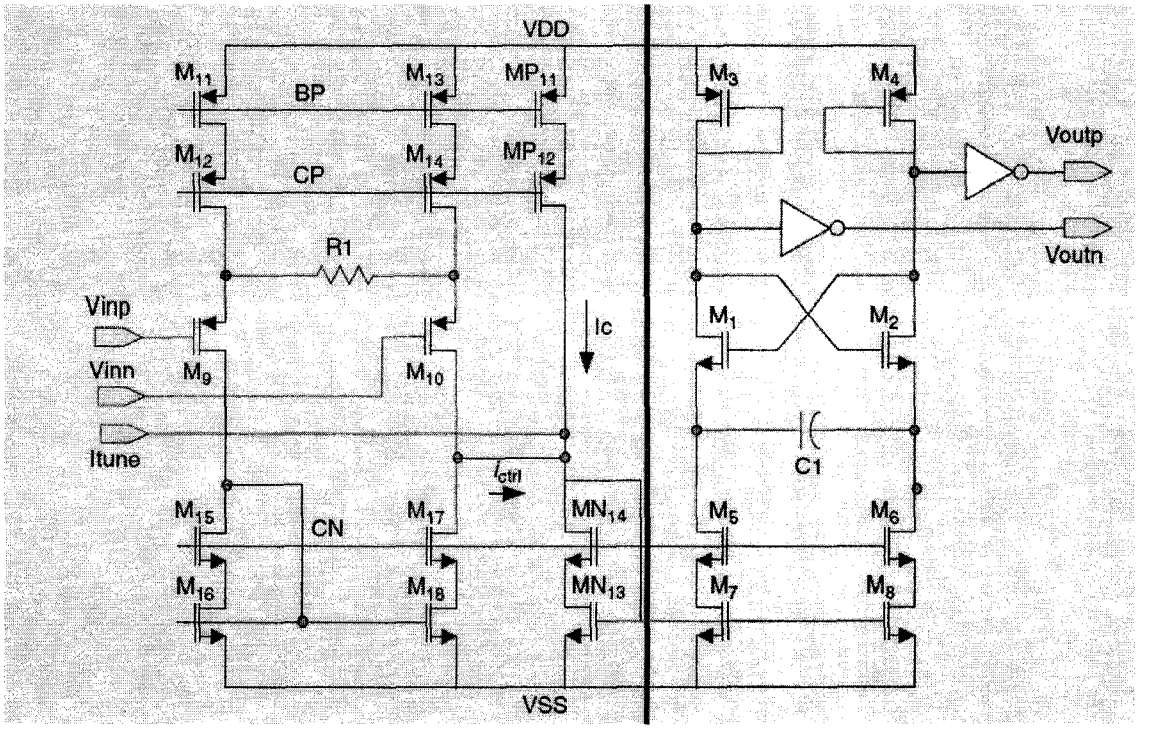

Figure 5.11 VCO circuit [35].

5.3.2.4 Phase Shifter (Quadrature Signal Generator)

As shown in Figure 5.8(b), there is a need to generate the quadrature of the oscillated signal in the lower branch of the demodulator. This task can be completed by a digital circuit consisting two D-flip flops as shown in Figure 5.12 [35]. The function of this circuit is to generate 90 degrees shift in phase of the input signal and convert the sine function to cosine function and vice versa. This is simply achieved by addition of a time delay in the function using D-flip flops. It should be noted that a reference with twice of

the carrier frequency has to be generated in the VCO with this circuit which results in a slightly more power consumption but still the best option for the desired application.

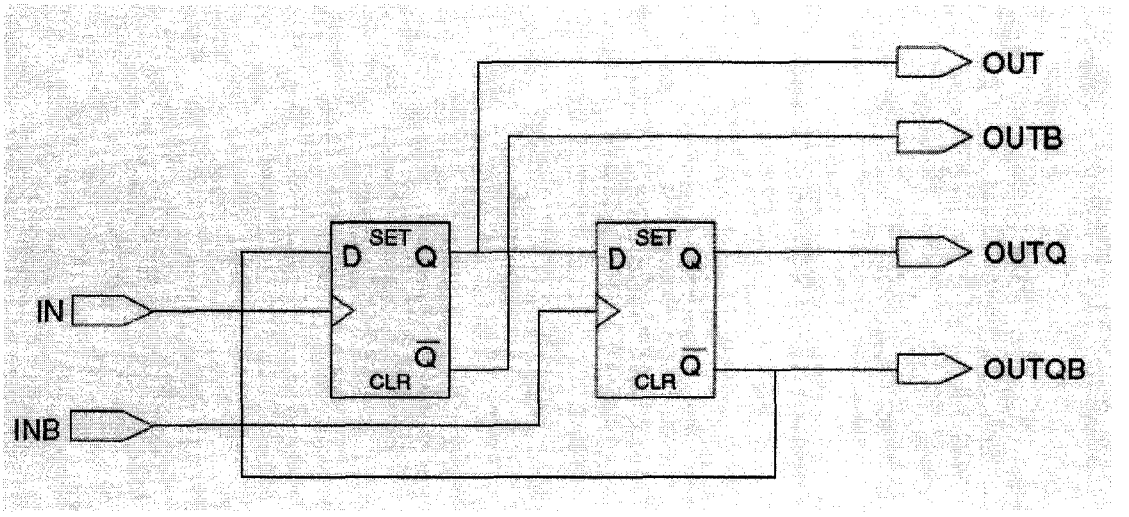

Figure 5.12 Phase detector and multiplier circuit [35].

5.4 Summary

In this chapter, an electrical engineering solution using circuit implementation for treatment of GERD has been proposed. The approach is based on the electrical stimulation of a sphincter located at the junction of the stomach and the esophagus in order to control the acid reflux. For the first time, a new idea for implementation of the approach using an electronic implantable device has been presented. Furthermore, a number of sample circuits for the implant structure from the literature have been described briefly. The objective has been to provide a framework for further research on the proposed idea of the implant for GERD treatment.

Chapter 6

Conclusions

6.1 Contributions

Esophageal motility disorders (EGMDs) correspond to a group of widespread diseases with a rapidly increasing prevalence rate in North America. The diagnosis of EGMDs can be tedious, time consuming, and technically challenging. This thesis attempted to address the challenges of EGMDs diagnosis through the use of signal processing methods. The ultimate goal has been to develop new computer-based approaches that:

i) Increase the accuracy of the diagnosis;

ii) Reduce the amount of time required for diagnosis;

iii) Enhance the ability of the experts in diagnosis.

In addition, a new circuit-based solution for treatment of GERD, *i.e.* the most common disease caused by EGMDs, using electrical neuro-stimulation methods is proposed. The main objective has been to provide a framework for further research regarding a potential GERD treatment based on electrical neuro-stimulation methods.

The desire for development of engineering techniques applicable to diagnosis and treatment of EGMDs demands for a basic knowledge about the esophagus physiology and its motility. As such, chapter 2 of this thesis was devoted to an overview of the medical aspect. This chapter included a brief description of the esophagus anatomy, an explanation of EGMDs causes, as well as a brief overview of GERD.

The key test for motility assessment of esophagus is EGM. EGM results are inspected visually by medical experts for diagnosis. However the visual inspection of the results by the doctors can be tedious due to the fact that the results are usually contaminated by noise and artifacts. As such, new signal processing-based approaches aiming at simplifying the EGMDs diagnosis are developed and described in chapters 3 and 4 of this thesis. In chapter 3, a signal processing technique *i.e.* WD, is applied to the filtering of the EGM data. In chapter 4, a new NPDT is applied to the de-noised EGM data leading to identification and extraction of diagnostically important information. Such information is used to generate a statistical model, which can classify the EGM patterns. The proposed approach is computationally effortless, thus making it suitable for real-time application. Experimental results using measured EGM data from patients is presented in

each chapter. In addition, the results of the proposed techniques are compared with those techniques from existing literature where applicable. Such comparisons show the advantages of the proposed approaches over the existing techniques.

In chapter 5, a new approach for treatment of GERD based on electrical neuro-stimulation methods has been proposed. The approach involves the design of an implantable device dedicated to electrical stimulation of a sphincter at the junction of the esophagus and the stomach. The proposed approach is an effective tool for GERD treatment compared to the existing surgical methods and may permanently cure GERD. The main structure of the implant system as well as a group of state-of-the-art analog circuits from existing literature have been described in order to provide a framework for the design and implementation of the idea.

6.2 Future Work

The proposed approaches for EGMDs diagnosis offer a scope for future work in terms of additions and improvements. Further research towards the development of more efficient techniques for filtering and detection of key EGM data can provide more practical tools for medical experts in EGMDs diagnosis. For instance, in case of WD filtering technique, further research towards development of a new optimum wavelet for the EGM data analysis to replace the symlets may increase efficiency and accuracy of the WD. In addition, in case of NPDT, the detection of EGM pulses can be improved by defining the algorithms that are more accurate/efficient in finding the CPs. Ultimately, the proposed SPM for EGM pulse modeling can be modified and completed through

addition of new features that take account of the EGM pulses' coordination in addition to the pulses' shape information.

The proposed approach for GERD treatment demands future work in terms of extensive study towards the implementation of the implant system. Such study may include the detailed analysis of the LES motor function along with the best ways of its stimulation, the development of control algorithms based on the defined responsibilities of the implant and the design of the specific circuits in the implant system.

REFERENCES

[1] M. Feldman, L.S. Friedman, L.J. Brandt, and M.H. Sleisenger, *Gastrointestinal and Liver Disease*, 8th ed., vol. 1, Philadelphia, PA: Saunders Elsevier, 2006, chapter 41, pp. 855-877.

[2] D.O. Castell and J.E. Richter, *The Esophagus*, 4th ed., Philadelphia, PA: Lippincott Williams & Wilkins, 2004, chapter 5, pp. 115-136.

[3] F.A. Granderath, T. Kamolz, and R. Pointner, *Gastroesophageal Reflux Disease*, 1st ed., Wien, Austria: Springer-Verlag, 2006, chapter 11, pp. 121-139.

[4] http://www.riversideonline.com/source/images/image_popup/ans7_esophagus.jpg

[5] http://www.gispecialists.net/images/art/stomach.gif

[6] H. Liang, Q. Lin, and J.D.Z. Chen, "Application of empirical mode decomposition to the analysis of esophageal manometric data in gastroesophageal reflux disease," *IEEE Trans. Biomed. Engg.*, vol. 52, no. 10, pp. 1692-1701, 2005.

[7] W. Qiao, H.H. Sun, W.Y. Chey, and K.Y. Lee, "Continous wavelet analysis as an aid in the representation and interpretation of electrogastrographic signals," *Proc. IEEE. Biomed. Engg. Conf.*, Dayton, OH, March 1996, pp.140-141.

[8] H. Liang and Z. Lin, "Stimulus artifact cancellation in the serosal recordings of gastric myoelectric activity using wavelet transforms," *IEEE Trans. Biomed. Engg.*, vol. 49, pp. 681-688, 2002.

[9] I. Daubechies, *Ten Lectures on Wavelets*, 2nd ed., Philadelphia, PA: Society for Industrial Mathematics, 1992, chapters 3-5, pp. 53-167.

[10] J.R. Smith, "Automatic analysis and detection of EEG spikes," *IEEE Trans. Biomed. Engg.*, vol. 21, no. 1, pp. 1-7, 1974.

[11] X. Yang and S.A. Shamma, "A totally automated system for the detection and classification of neural spikes," *IEEE Trans. Biomed. Engg.*, vol. 35, no. 10, pp. 806-816, 1988.

[12] M.G. Frei, R.L. Davidchack, and I. Osorio, "Least squares acceleration filtering for the estimation of signal derivatives and sharpness at extrema," *IEEE Trans. Biomed. Engg.*, vol. 46, no. 8, pp. 971-977, 1999.

[13] H.S. Bokil, B. Pesaran, R.A. Andersen, and P.P. Mitra, "A method for detection and classification of events in neural activity," *IEEE Trans. Biomed. Engg.*, vol. 53, no. 8, pp. 1678-1687, 2006.

[14] J. Muthuswamy, D.L. Sherman, and N.V. Thakor, "Higher-order spectral analysis of burst patterns in EEG," *IEEE Trans. Biomed. Engg.*, vol. 46, no. 1, pp. 92-99, 1999.

[15] T.S. Parker and L.O. Chua, *Practical Numerical Algorithems for Chaotic systems*, 1st ed., New York, NY: Springer-Verlag, 1989, chapters 2-5, pp. 38-348.

[16] J.J. Gray, *Linear Differential Equations and Group Theory from Riemann to Poincaré*, 2nd ed., Boston, MA: Birkhauser, 2000, chapter 6, pp. 173-221.

[17] E.W. Cheney and D.R. Kincaid, *Numerical Mathematics and Computing*, 4th ed., Pacific Grove, CA: Brooks Cole Pub. Co., 1999, chapter 10, pp. 453-521.

[18] J. Gotman and P. Gloor, "Automatic recognition and quantification of interictal epileptic activity in the human scalp EEG," *Electroencephalography and Clinical Neurophysiology*, vol. 41, pp.513-529, 1976.

[19] J.F. Kaiser, "On a simple algorithm to calculate the 'energy' of a signal," *Proc. IEEE. Int. Conf. ICASSP*, Albuquerque, NM, April 2007, pp. 381-384.

[20] E.I. Plotkin and M.N.S. Swamy, "Nonlinear signal processing based on parameter invariant moving average modeling," *Proc. CCECE*, Toronto, Canada, Sept. 1992, pp. TM3.11.1-TM3.11.4.

[21] S.H. Strogatz, *Nonlinear Dynamics and Chaos: with Applications to Physics, Biology, Chemistry, and Engineering*, 1st ed., vol. 1, Reading, MA: Addison-Wesley, 1994, chapters 1-10, pp. 1-398.

[22] D. Singh and K. Vinod "Effect of RR segment duration on short-term HRV assessment using Poincare plot," *Proc. IEEE. Int. Conf. ICISIP*, Chennai, India, Jan. 2005, pp. 430-434.

[23] M. Brennan, M. Palaniswami, and P. Kamen, "Do existing measures of poincaré plot geometry reflect nonlinear features of heart rate variability?," *IEEE Trans. Biomed. Engg.*, vol. 48, no. 11, pp. 1342-1346, 2001.

[24] W.E. Finn and P.G. LoPresti, *Handbook of Neuroprosthetic Methods*, 1st ed., Boca Raton, FL: CRC Press, 2003, chapters 4-7, pp. 75-195.

[25] S. Boyer, M. Sawan, M. Abdel-Gawad, S. Robin, and M.M. Elhilali, "Implantable selective stimulator to improve bladder voiding: Design and chronic experiments on dogs," *IEEE Trans. Rehabilitation Engg.*, vol. 8, no. 4, pp. 464-470, 2000.

[26] Y. Hu, M. Sawan, and M.N. El-Gamal, "A power recovery strategy dedicated to implantable applications," *Proc. IEEE. Int. Conf. ICECS*, Sharjah, UAE, Dec. 2003, pp.1212-1215.

[27] A. M. Sodagar, K. Najafi, K. D. Wise, and M. Ghovanloo, "Fully-integrated CMOS power regulator for telemetry-powered implantable biomedical

microsystems," *Proc. IEEE. Int. Conf. CICC*, San Jose, CA, Sept. 2006, pp. 659-662.

[28] G. J. Suaning and N.H. Lovell, "CMOS neurostimulation ASIC with 100 channels, scaleable output, and bidirectional radio-frequency telemetry," *IEEE Trans. Biomed. Engg.*, vol. 48, no. 2, pp. 248–260, 2001.

[29] W. Liu, et al., "A neuron-stimulus chip with telemetry unit for retinal prosthetic device," *IEEE J. Solid-State Circuits*, vol. 35, no 10, pp. 1487–1497, 2000.

[30] T. Akin, K. Najafi, and R.M. Bradley, "A wireless implantable multichannel digital neural recording system for a micromachined sieve electrode," *IEEE J. Solid-State Circuits*, vol. 33, no 1, pp. 109–118, 1998.

[31] J. Parramon, et al., "ASIC-based battery less implantable telemetry microsystem for recording purposes," *Proc. IEEE. EMBS Int. Conf.*, Chicago, IL, Nov. 1997, pp. 2225–2228.

[32] G. Gunnar, E. Bruun, and H. Morten, "A Chip for an Implantable Neural Stimulator," *Journal of Analog Integrated Circuits and Signal Processing*, vol. 22, pp. 81–89, 1999.

[33] B. Smith, et al., "An externally powered, multichannel, implantable stimulator-telemeter for control of paralyzed muscle," *IEEE Trans. Biomed. Engg.*, vol. 45, no 4, pp. 463–475, 1998.

[34] Y. Hu and M. Sawan, "A fully integrated low-power BPSK demodulator for implantable medical devices," *IEEE Trans. Circuits and Systems I*, vol. 52, no. 12, pp. 2552-2562, 2005.

[35] M. Sawan, Y. Hu, and J. Coulombe, "Wireless smart implants dedicated to multichannel monitoring and microstimulation," *IEEE Circuits and Systems Magazine*, vol. 5, no. 1, pp. 21-39, 2005.